Chapter 3

Optimization of isolated annular fin

In this chapter, the analysis of the isolated annular fins undertaken in this thesis, is described, involving all the parameters and variables needed for the formulation. The problem is also represented diagrammatically with the help of figures. The heat transfer as well as thermal stress model considered in this problem, is also illustrated here. Then, the mathematical formulation is given to evaluate the different design variables through an optimizing algorithm.

As thermal conductivity k varies linearly with temperature T_i in most of the fin materials, the relationship between the thermal conductivity k and temperature T_i, given by Eq. (3.1), is adopted here. [86].

$$k = k_a \{1 + \beta (T_i - T_\infty)\} \tag{3.1}$$

In Eq. (3.1), T_∞ is ambient temperature, k_a is the value of k at T_∞, and β is a parameter that controls the variation in k. Further, $T_i = T$ in uniform and continuously varying thickness fins, while i in T_i indicates the steps in the fin with step change in thickness ($i = 1$ in the first step and $i = 2$ in the second step).

The thickness of the fin is assumed to be very small, so that the heat transfer by conduction in the radial direction can be treated as a one-dimensional flow without any significant difference. The heat losses from the fin surface to the surrounding fluid are assumed to be taken place by natural convection and radiation. The other assumptions are steady state, constant convection heat transfer coefficient, h (though in real case convection heat transfer coefficient varies in the direction of fluid flow, it is assume constant here mainly for the purpose of simplifying the analysis) and no internal heat generation. Considering a constant temperature T_b at the base of the fin, one-dimensional steady-state analysis for the studied fin profiles based on Eq. (3.1) are discussed as follows:

3.1 Stepped fin

The problem discussed here is a two-stepped rectangular cross-sectional annular fin attached to a heat exchanger of cylindrical primary surface.

A schematic diagram of the two-stepped rectangular cross-sectional annular fin is shown in Fig. 3.1. The inner and outer radii of the fin are r_{b} and r_o respectively, while the radius at the point of step change in thickness is r_1. The cross-sectional half-thickness of the base and that of the tip of the fin are t_1 and t_2, respectively.

3.1.1 Formulation for heat transfer equation

Based on conditions of Eq. (3.1), the steady state energy balance governing equation for the fin can be expressed by Eq. (3.2).

$$\left.\begin{aligned} &\tfrac{d}{dr}\left[r\left\{1+\beta\left(T_i-T_\infty\right)\right\}\tfrac{dT_i}{dr}\right]-\tfrac{hr}{k_a t_i}\left\{T_i-T_\infty+\tfrac{\sigma\epsilon\left({T_i}^4-T_\infty^4\right)}{h}\right\}=0 \\ \text{where,}\quad &r_{\mathrm{b}}\le r\le r_1\ ;\quad \text{for}\quad i=1 \\ &r_1\le r\le r_o\ ;\quad \text{for}\quad i=2 \end{aligned}\right\} \tag{3.2}$$

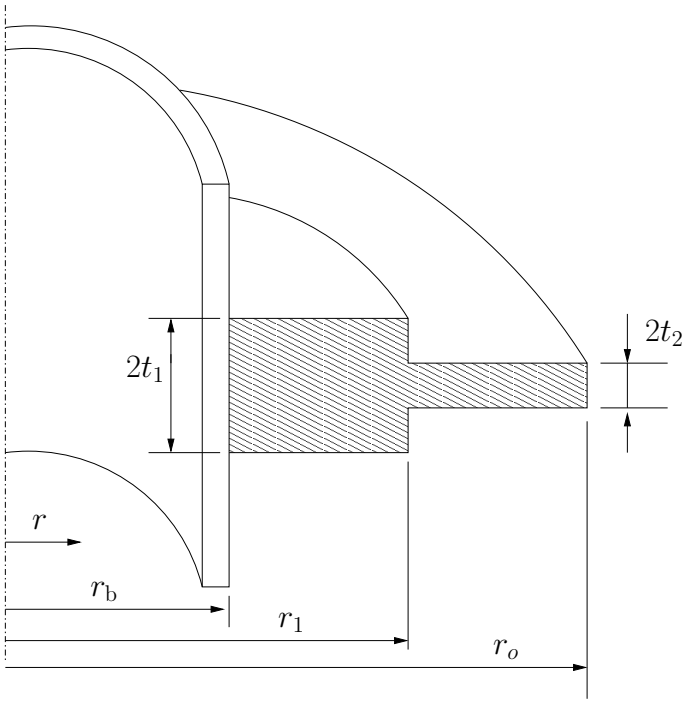

Figure 3.1: Schematic diagram of two-stepped annular fin.

In this study, the base of the fin (i.e, T_b) is considered to be at constant temperature and heat transfer by both convection and radiation is allowed through the tip of the fin to the surrounding. Also, since the continuity of temperature as well as energy balance must exist at the interface between the thick and thin sections of the fin, Eq. (3.2) is subjected to the boundary conditions given by Eq. (3.3).

$$T_1 = \begin{cases} T_b \ ; & \text{if} \quad r = r_b \\ T_2 \ ; & \text{if} \quad r = r_1 \end{cases} \tag{3.3a}$$

$$-k_a \left\{1 + \beta \left(T_2 - T_\infty\right)\right\} \frac{dT_2}{dr} = h \left(T_2 - T_\infty\right) + \sigma\epsilon \left(T_2^4 - T_\infty^4\right) \ ; \quad \text{at} \quad r = r_o \tag{3.3b}$$

$$\begin{aligned} -t_1 k_a \left\{1 + \beta \left(T_1 - T_\infty\right)\right\} \frac{dT_1}{dr} = & - t_2 k_a \left\{1 + \beta \left(T_2 - T_\infty\right)\right\} \frac{dT_2}{dr} \\ & + h_s \left(t_1 - t_2\right) \left\{T_1 - T_\infty + \frac{\sigma\epsilon \left(T_1^4 - T_\infty^4\right)}{h_s}\right\} \ ; \ \text{at } r = r_1 \end{aligned} \tag{3.3c}$$

The temperature distribution and fin dimensions shown in Fig. 3.1 are normal-

ized, as given in Eq. (3.4), by defining some dimensionless parameters.

$$\left.\begin{array}{llllll} R_1 = \frac{r_\mathrm{b}}{r_o} & R_o = \frac{r_1}{r_o} & R = \frac{r}{r_o} & & \\ y_s = \frac{t_2}{t_1} & \xi = \frac{t_1}{r_\mathrm{b}} & \mathrm{Bi} = \frac{hr_\mathrm{b}}{k_a} & \mathrm{Bi}_s = \frac{h_s r_\mathrm{b}}{k_a} & \\ \theta = \frac{T_1 - T_\infty}{T_b - T_\infty} & \phi = \frac{T_2 - T_\infty}{T_b - T_\infty} & \delta = \frac{T_\infty}{T_b - T_\infty} & & \\ R_f = \frac{\sigma\epsilon(T_b - T_\infty)^3}{h} & R_{f_s} = \frac{\sigma\epsilon(T_b - T_\infty)^3}{h_s} & \alpha = (T_b - T_\infty)\,\beta & & \end{array}\right\} \tag{3.4}$$

In terms of the dimensionless parameters defined in Eq. (3.4), Eqs. (3.2) and (3.3) are expressed in non-dimensional forms as in Eqs. (3.5) and (3.6), respectively.

$$\left.\begin{array}{ll} & (1+\alpha\kappa)\frac{d^2\kappa}{dR^2} + \left\{\alpha\frac{d\kappa}{dR} + \frac{1}{R}(1+\alpha\kappa)\right\}\frac{d\kappa}{dR} \\ & -Z^2\kappa\left\{1 + R_f\left(4\delta^3 + 6\delta^2\kappa + 4\delta\kappa^2 + \kappa^3\right)\right\} = 0 \\ \text{where,} & \kappa = \theta\ ,\ Z = \frac{Z_0}{R_1}\ ; \quad \text{if} \quad R_1 \le R \le R_o \\ & \kappa = \phi\ ,\ Z = \frac{Z_1}{\sqrt{y_s}}\ ; \quad \text{if} \quad R_o \le R \le 1 \\ & Z_0 = \sqrt{\frac{\mathrm{Bi}}{\xi}} \\ & Z_1 = \frac{Z_0}{R_1} \end{array}\right\} \tag{3.5}$$

$$\theta = \begin{cases} 1\ ; & \text{at} \quad R = R_1 \\ \phi\ ; & \text{at} \quad R = R_o \end{cases} \tag{3.6a}$$

$$-\left(1+\alpha\phi\right)\frac{d\phi}{dR} = \frac{\mathrm{Bi}}{R_1}\phi\left\{1 + R_f\left(4\delta^3 + 6\delta^2\phi + 4\delta\phi^2 + \phi^3\right)\right\}\ ; \quad \text{at} \quad R = 1 \tag{3.6b}$$

$$\begin{aligned} R_1\left(1+\alpha\theta\right)\frac{d\theta}{dR} =& y_s R_1\left(1+\alpha\phi\right)\frac{d\phi}{dR} \\ & - \mathrm{Bi}_s\left(1-y_s\right)\theta\left\{1 + R_{f_s}\left(4\delta^3 + 6\delta^2\theta + 4\delta\theta^2 + \theta^3\right)\right\}\ ;\ \text{at}\ R = R_o \end{aligned} \tag{3.6c}$$

3.1.2 Optimization modeling

In the present study, the performance of the studied two-stepped rectangular cross-sectional annular fin is evaluated in different combinations of five functions, which are heat transfer rate (f_1), fin volume (f_2), fin heat transfer surface area (f_3), fin efficiency (f_4), and fin effectiveness (f_5). Further, as shown in Fig. 3.1, the geometry of the fin can be defined in terms of only four independent parameters, which are fin radius at the point of step change in thickness (r_1), outer radius of the fin (r_o), cross-sectional half thickness of the thick (first) step of the fin (t_1), and cross-sectional half thickness of the thin (second) step of the fin (t_2). Therefore, it is clear that a change in the value of any of these four independent parameters will lead to a new design with different values of the five performance functions of the fin. Accordingly, treating these four independent geometric parameters as the design variables and the five performance functions as the objective functions, the considered fin design can be modeled as a multi-objective optimization problem as given by Eq. (3.7).

$$\left.\begin{array}{rrcl} \text{Determine} & \boldsymbol{x} & \equiv & (r_1, r_o, t_1, t_2)^{\mathrm{T}} \\ \text{to maximize} & \boldsymbol{z}(\boldsymbol{x}) & \equiv & \{f_1(\boldsymbol{x}), f_4(\boldsymbol{x}), f_5(\boldsymbol{x})\} \\ \text{minimize} & \boldsymbol{f}(\boldsymbol{x}) & \equiv & \{f_2(\boldsymbol{x}), f_3(\boldsymbol{x})\} \\ \text{subject to} & g_1(\boldsymbol{x}) & \equiv & r_1 > r_{\mathrm{b}} \\ & g_2(\boldsymbol{x}) & \equiv & r_o > r_1 \\ & g_3(\boldsymbol{x}) & \equiv & t_1 > t_2 \\ & & & r_1, r_o, t_1, t_2 \geq 0 \ . \end{array}\right\} \tag{3.7}$$

In Eq. (3.7), constraints $g_1(\boldsymbol{x})$ and $g_2(\boldsymbol{x})$ ensure the existence of two steps (sections) in the fin, and constraint $g_3(\boldsymbol{x})$ ensures that they (i.e., the two fin steps) are of different cross-sectional thicknesses, thus resulting in a two-stepped rectangular cross-sectional fin. On the other hand, the last line in Eq. (3.7) makes the design variables non-negative (in practice, positive). Further, $r_o \ggg 2t_b$ (i.e., the outer radius of the fin is sufficiently larger than its thickness at the base) may be maintained to make the fin thin enough, so that it can be studied under one-dimensional heat

conduction in the radial direction only. The five objective functions $f_1(\boldsymbol{x})$–$f_5(\boldsymbol{x})$ in Eq. (3.7) are the heat transfer rate, fin volume, fin heat transfer surface area, fin efficiency and fin effectiveness, respectively. The maximization of $f_1(\boldsymbol{x})$, $f_4(\boldsymbol{x})$ and $f_5(\boldsymbol{x})$ improves the overall thermal performance of the fin, while the minimization of $f_2(\boldsymbol{x})$ and $f_3(\boldsymbol{x})$ reduces the fin material and space cost. In terms of the notations and formulation for heat transfer equation of the fin, presented in Section 3.1.1, these objective functions can be defined by Eq. (3.8).

$$f_1(\boldsymbol{x}) = -kA_b \left.\frac{dT_1}{dr}\right|_{r=r_\mathrm{b}} \tag{3.8a}$$

$$f_2(\boldsymbol{x}) = 2\pi \left\{ t_1 \left(r_1^2 - r_\mathrm{b}^2\right) + t_2 \left(r_o^2 - r_1^2\right) \right\} \tag{3.8b}$$

$$f_3(\boldsymbol{x}) = 2\pi \left(r_o^2 - r_\mathrm{b}^2\right) + 4\pi \left\{ r_1 \left(t_1 - t_2\right) + r_o t_2 \right\} \tag{3.8c}$$

$$f_4(\boldsymbol{x}) = \frac{f_1(\boldsymbol{x})}{h f_3(\boldsymbol{x}) \left(T_b - T_\infty\right) + \sigma \epsilon f_3(\boldsymbol{x}) \left(T_b^4 - T_\infty^4\right)} \tag{3.8d}$$

$$f_5(\boldsymbol{x}) = \frac{f_1(\boldsymbol{x})}{h A_b \left(T_b - T_\infty\right) + \sigma \epsilon A_b \left(T_b^4 - T_\infty^4\right)} \tag{3.8e}$$

where, $A_b = 4\pi r_b t_1$

3.1.3 Solution procedure

The fin design problem, formulated in Eq. (3.7) as a multi-objective optimization model, is solved using a very popular and widely applied multi-objective genetic algorithm, namely nondominated sorting genetic algorithm II (NSGA-II) proposed by Deb et al. [23]. The working steps of (NSGA-II) in the context of the present study is summarized in Section A.2.4.

The heat transfer rate, $f_1(\boldsymbol{x})$, is evaluated numerically by solving the problem governing Eq. (3.5) along with its initial and boundary conditions given by Eq. (3.6). The non-dimensional temperature distribution (θ, ϕ) along the length of the fin is first evaluated by solving Eqs. (3.5) and (3.6) using the hybrid spline difference

method (HSDM) proposed by Wang et al. [83–86]. The computational process of HSDM is similar to those of the finite difference methods, but an accuracy of fourth order can be achieved in HSDM while evaluating the first-order and second-order derivative functions. Also, sufficiently large number of grid points and low values in termination criteria of the iteration process are considered in order to obtain results with higher accuracy. Validating the performance through the predicted tip temperature and fin efficiency as shown in Table 3.1, it is found that the numerical results

Table 3.1: Error analysis of HSDM in case of annular stepped fin (design condition: $R_1 = 0.5,\ R_2 = 0.75,\ y_s = 0.5,\ Bi_s = 0.0$)

Z_0	(a) Non-dimensional temperature at the tip			(b) Fin Efficiency		
	Exact [44]	HSDM (present work)	% Error	Exact [44]	HSDM (present work)	% Error
0.1	0.99231	0.99231	0.0	0.9947	0.9947	0.0
0.2	0.96981	0.96981	0.0	0.9793	0.9793	0.0
0.3	0.93416	0.93416	0.0	0.9549	0.9549	0.0
0.4	0.88778	0.88778	0.0	0.9229	0.9229	0.0
0.5	0.83348	0.83348	0.0	0.8854	0.8854	0.0
0.6	0.77417	0.77417	0.0	0.8441	0.8441	0.0
0.7	0.71245	0.71245	0.0	0.8009	0.8009	0.0
0.8	0.65054	0.65054	0.0	0.7572	0.7572	0.0
0.9	0.59016	0.59016	0.0	0.7141	0.7141	0.0
1.0	0.53253	0.53253	0.0	0.6725	0.6725	0.0

of HSDM exactly match with the deterministic exact results reported by Kundu et al. [44], thus demonstrating the accuracy of HSDM as well as the correctness of the algorithm used for solving the direct problem. The discrete relationships with the concept of HSDM are given in Eq. (A.9).

The detail procedure for evaluating $f_1(\boldsymbol{x})$ in Step (3) of NSGA-II, through the HSDM scheme expressed by Eq. (A.9), is as follows:

(a) Discretize Eqs. (3.5) and (3.6) as in Eq. (A.9).

(b) Evaluate p_n $(n = 0, 1, \ldots, N)$ by solving the discretized form of Eqs. (3.5) and (3.6) using the variant of the Thomas algorithm proposed by Martin and Boyd [64].

(c) At all the grid points, evaluate the dimensionless temperature distribution and their derivatives up to the second order, i.e., θ_n, ϕ_n, θ'_n, ϕ'_n, θ''_n and ϕ''_n using the values of p_n in Eq. (A.9).

(d) Evaluate the temperature gradient at the base of the fin, i.e., $\frac{dT_1}{dr}\big|_{r=r_b}$, from the dimensionless temperature gradient θ'_o at the base of the fin.

(e) Evaluate $f_1(\boldsymbol{x})$ using the value of $\frac{dT}{dr}\big|_{r=r_b}$ in Eq. (3.8a).

3.1.4 Numerical experimentation and discussion

In the present study, a rectangular cross-sectional two-stepped annular fin, having constant base temperature and variable heat conductivity, is studied in a convective and radiative environment. The considered operating conditions, thermal properties of the fin material, and fin geometry with reference to Fig. 3.1 are listed in Table 3.2,

Table 3.2: Operating conditions, fin material properties, and fin geometry for annular stepped fin.

Parameter	Value/ range of value
Ambient temperature, T_∞	300 K
Fin temperature at the base, T_b	600 K
Convective heat transfer coefficient on the fin surface, h	50 W/m^{2}K
Convective heat transfer coefficient on the step surface, h_s	50 W/m^{2}K
Thermal conductivity of the fin material at T_∞, k_a	186 W/mK
Parameter for variable thermal conductivity, β	-0.00018 K^{-1}
Emissivity of the fin material, ϵ	0.8
Base radius, r_b	2.0 cm
Radius of step change in thickness, r_1	2.5–6.0 cm
Outer radius, r_o	2.5–6.0 cm
Half thickness of the first step, t_1	0.01–0.2 cm
Half thickness of the second step, t_2	0.01–0.2 cm

while the user defined algorithmic parameter settings for NSGA-II are fixed based on some trial runs as given in Table 3.3. With these sets of input values and randomly

Table 3.3: User defined parameter setting in the context of NSGA-II.

Parameter	Value/ range of value
Population size	100
Number of generations	400
Crossover probability	90%
Distribution index for the SBX crossover operator	10
Mutation probability	0–1%
Distribution index for the polynomial mutation operator	100

generated NSGA-II population, the fin design optimization problem formulated in Eq. (3.7) is studied under two scenarios of the considered five objective functions f_1–f_5 given by Eq. (3.8). In the first scenario, the objective functions are optimized

in various pairs, while all the five objective functions are optimized simultaneously in the second scenario.

3.1.4.1 Scenario I

Initially the fin configuration optimization problem is studied for maximizing the heat transfer rate f_1 and minimizing the fin volume f_2. The obtained final Pareto front, containing the set of trade-off solutions in terms of f_1 and f_2, is shown in Fig. 3.2(a). It clearly reveals the conflicting nature between the heat transfer rate

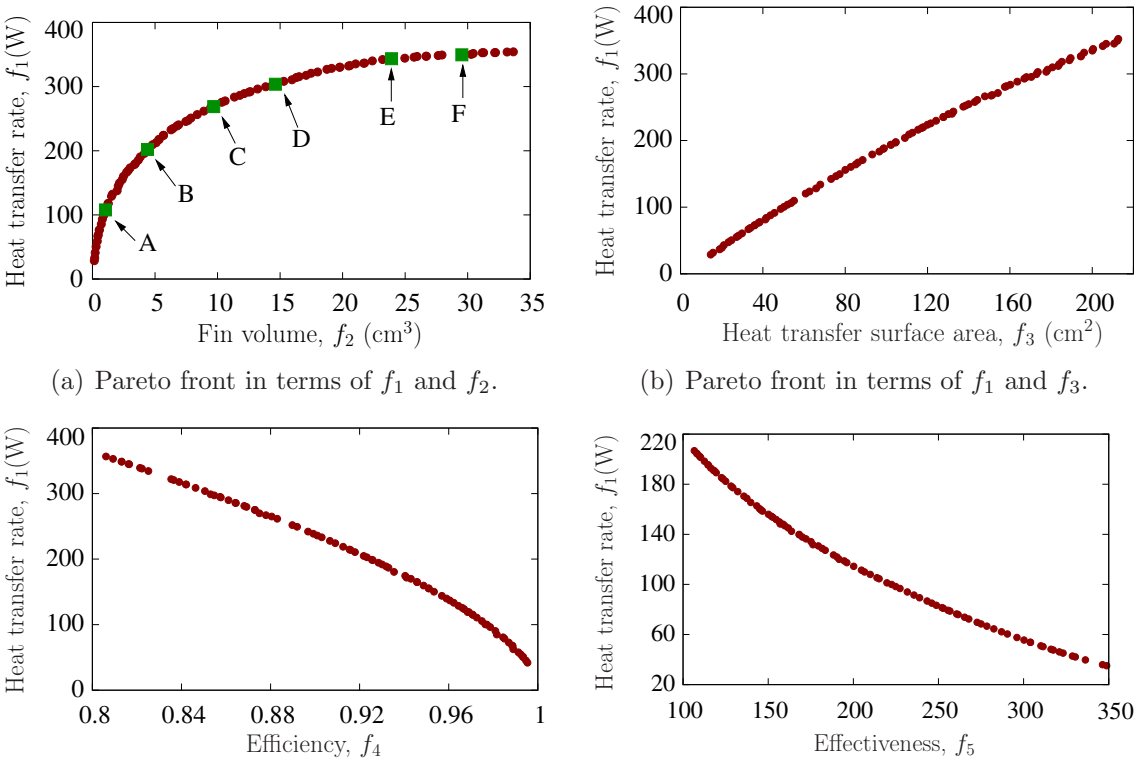

(a) Pareto front in terms of f_1 and f_2.

(b) Pareto front in terms of f_1 and f_3.

(c) Pareto front in terms of f_1 and f_4.

(d) Pareto front in terms of f_1 and f_5.

Figure 3.2: Pareto fronts for pairwise objective functions.

and the fin volume, i.e., one objective cannot be improved without degrading the other at least by some amount. Six selective efficient fin geometries, corresponding to trade-off solutions A–F of Fig. 3.2(a), are shown in Fig. 3.3, where the pattern of geometric variations in the fin configurations is noticeable. For these configurations, the values of other three objective functions, i.e., f_3–f_5, are also computed and shown in Fig. 3.3 along with the design parameter values. The notations for design

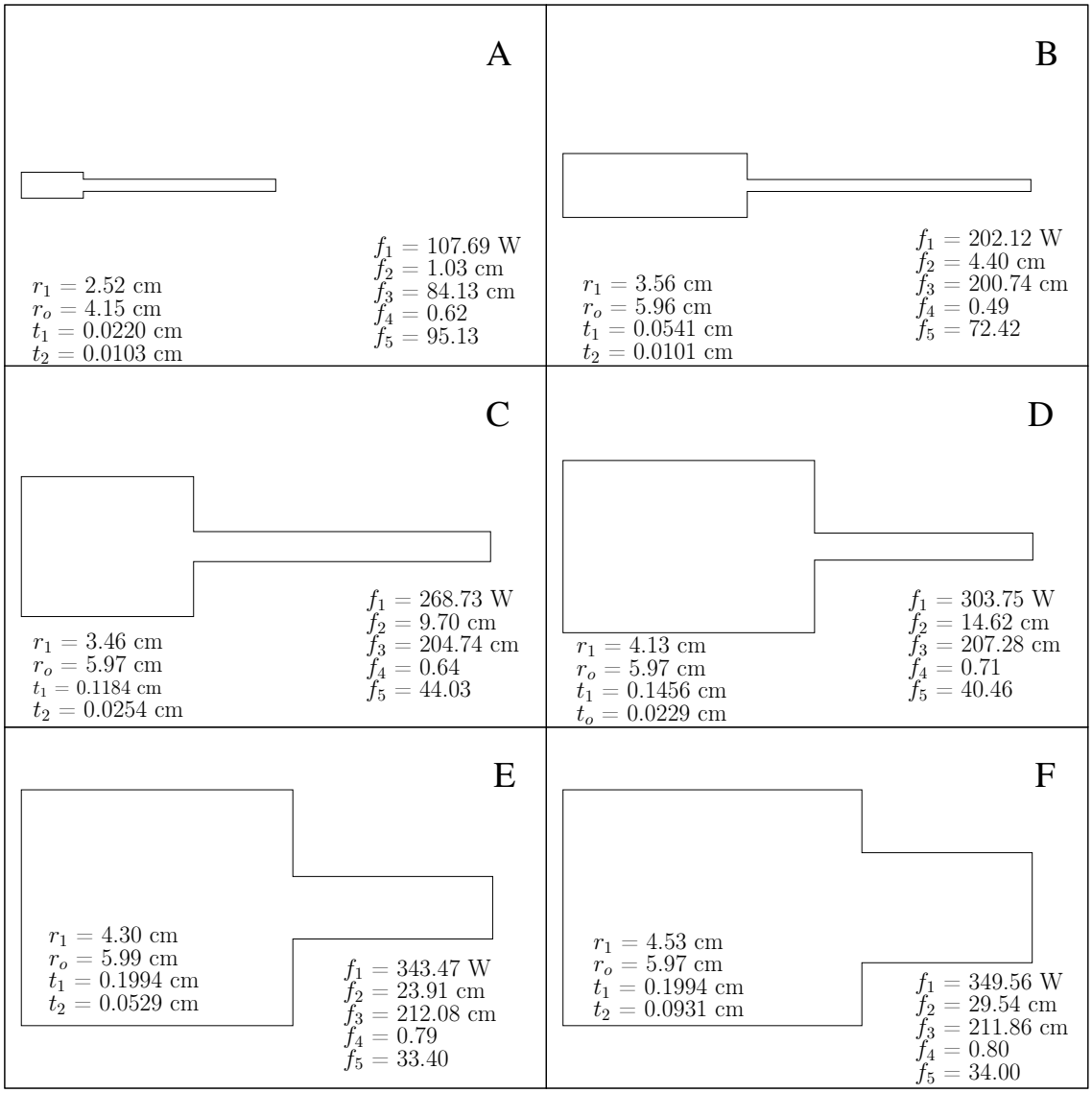

Figure 3.3: Selective efficient fin geometries (corresponding to trade-off solutions A–F of Fig. 3.2(a).)

parameters in Fig. 3.3 are as per those used in Fig. 3.1. From Fig. 3.3, it is observed that the patterns of variations of f_3–f_5 with those of f_1 and f_2 are not very clear.

It is to be mentioned that in some applications (such as those pertaining to aerospace, electronic components, heat exchangers in vessels, etc.), the weight or the available space is a major design consideration, thus making fin volume (f_2) and fin heat transfer surface area (f_3) an important parameter to be optimized. It is also desirable for a fin to perform at its maximum capacity, i.e., at the ideal situation with the whole fin at its base temperature. However, because of the thermal resistance to conduction, the temperature gradually decreases along the radial direction of the

fin, causing the fin performance to fall from its ideal situation and subsequently the utilization of the fin material in an inefficient manner. Hence, if the economic aspect of the fin material is to be taken into account, the fin efficiency (i.e., f_4) becomes an important consideration in optimization of annular fins. On the other hand, the fin effectiveness (f_5) also becomes an important parameter to be optimized in the case of constrained surface area of the body to which the fin is attached. Hence, although the fin volume (i.e., f_2), the fin heat transfer surface area (i.e., f_3) and the fin performance factors (i.e., f_4 and f_5) are desirable to be optimum in a real life situation, optimum values of some of these objectives may be more important than others depending upon the availability of resources.

In view of above, the fin design optimization problem is studied in the second step for maximizing the heat transfer rate f_1 separately with minimizing the fin heat transfer surface area f_3, maximizing the fin efficiency f_4, and maximizing the fin effectiveness f_5, and the obtained Pareto fronts are shown in Figs. 3.2(b)–3.2(d), respectively. The Pareto front in Fig. 3.2(b) shows that the heat transfer rate f_1 conflicts with the fin heat transfer surface area f_3 also, i.e., an improvement in f_1 will degrade f_3 by some amount and *vice-versa*. Further, it can be noticed in Fig. 3.3 that the heat transfer rate gradually increases with increasing fin volume. Accordingly, since both the fin volume and fin heat transfer surface area are sought to be minimized against maximizing the heat transfer rate, it can be concluded that the fin volume and fin heat transfer surface area are not conflicting but correlated to some extent, i.e., both will be optimized (improved or degraded) simultaneously. Next studying the Pareto fronts in Figs. 3.2(c) and 3.2(d), it is observed the heat transfer rate f_1 conflicts with the fin efficiency f_4 and fin effectiveness f_5 also, i.e., a higher heat transfer rate will reduce both the fin efficiency and fin effectiveness. However, unlike the cases of the fin volume and fin heat transfer surface area, the trends of variation of the fin efficiency and fin effectiveness against the heat transfer rate are different. Therefore, finally the variation of the fin efficiency f_4 against the fin effectiveness f_5 is studied by taking them as two maximizing objective functions of the fin design problem. The obtained Pareto front is shown in Fig. 3.4, which depicts that the fin efficiency conflicts with the fin effectiveness. It may be noted

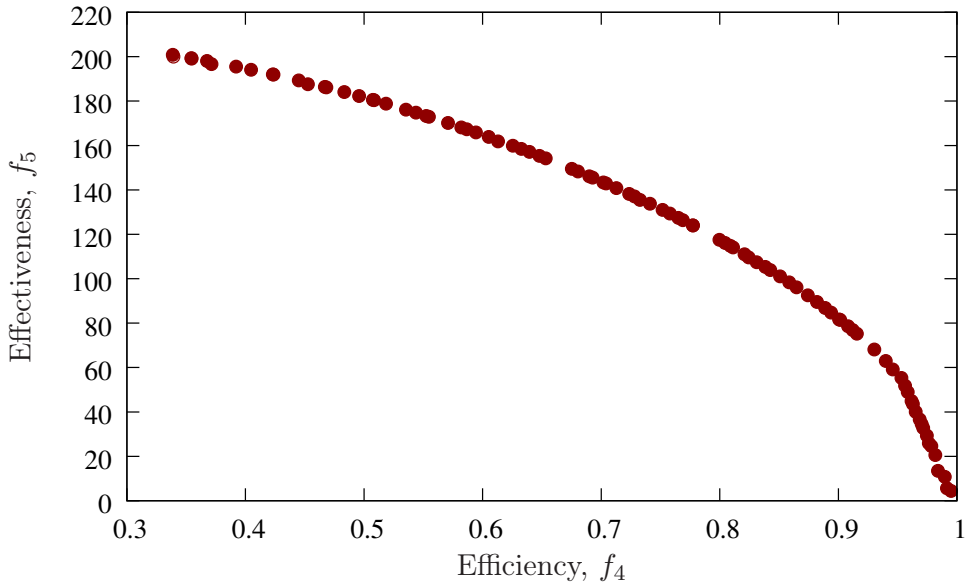

Figure 3.4: Pareto front of fin efficiency versus fin effectiveness.

that the fin efficiency is the ratio of the actual heat transfer rate from the fin to the ideal heat transfer rate with the entire fin surface at the base temperature, while the fin effectiveness is the ratio of the actual heat transfer rate from the fin to the heat transfer rate through the base area without any fin.

3.1.4.2 Scenario II

Studying pair-wise separately, it is observed in Section 3.1.4.1 that the variations of the objective functions are different, leading to no common pattern of the heat transfer rate. Therefore, all the five considered objective functions, i.e., f_1–f_5 given by Eq. (3.8), are optimized here simultaneously in order to arrive at a general scenario. Since a plot of more than three dimensions can neither be visualized directly nor analyzed effectively on a two-dimensional page, the obtained five-dimensional Pareto front is plotted in a parallel coordinate system as shown in Fig. 3.5, in which an objective function of interest is plotted in one of a series of parallel coordinate axes each of equal length [88]. The objective functions are marked here along the horizontal axis, and their values for different solutions are shown along the corresponding parallel vertical axes. Each crossing line in Fig. 3.5 represents a solution of the Pareto front, connecting the objective values of the solution on the respective

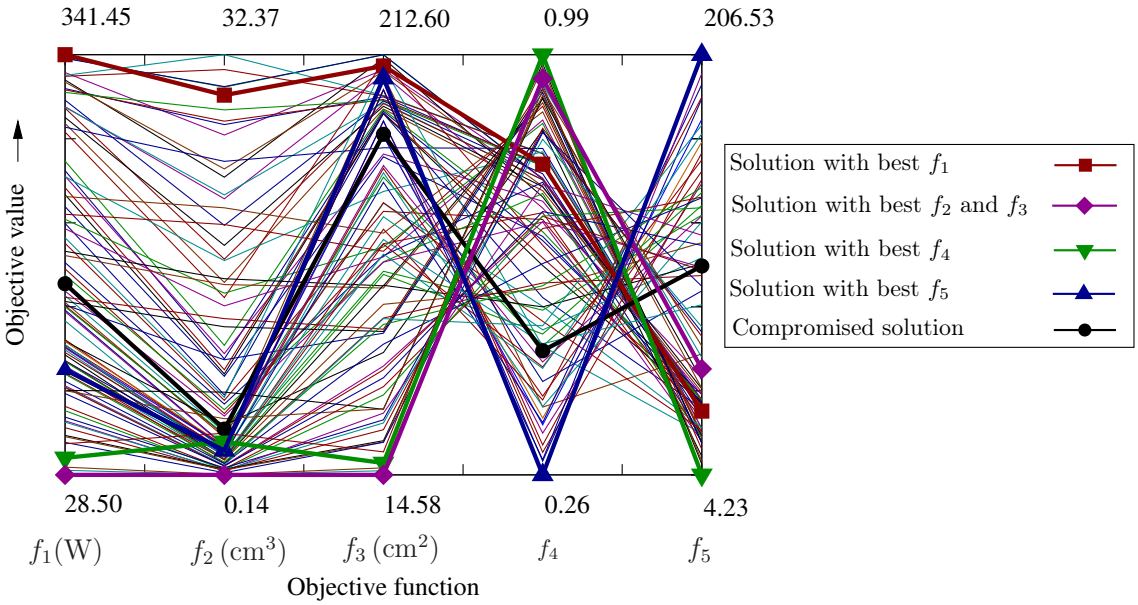

Figure 3.5: Five-dimensional Pareto front in two-dimensional parallel coordinate system.

parallel vertical axes. Accordingly, the conflicting objective values of any solution can be noticed in Fig. 3.5. For example, the solution corresponding to the maximum heat transfer rate bears very high fin volume and fin heat transfer surface area, and a moderately high fin efficiency, while a very low fin effectiveness.

The fact that in real life scenario, all the objective functions are desirable to be optimum justifies the need for optimizing all the objective functions simultaneously. Further, since the single plot of the Pareto front in Fig. 3.5 is able to show clearly the relationships of any objective function with the remaining four, a designer can enjoy the flexibility of adopting a compromise solution based upon the accessibility and practicability of information and resources available for the problem at hand. Such a compromise solution is also shown in Fig. 3.5, which bears some balanced values of the considered five objective functions.

3.1.5 Sensitivity analysis

Finally, sensitivity analysis is performed in order to study the influence of each design variable on the heat transfer rate. For this purpose, an arbitrary intermediate

solution is chosen from the Pareto front shown in Fig. 3.2(a). The solution has optimal objective values of $f_1^* = 178.46$ W and $f_2^* = 3.36$ cm^3, and the corresponding efficient fin geometry as $r_1^* = 3.35$ cm, $r_o^* = 5.11$ cm, $t_1^* = 0.05$ cm and $t_2^* = 0.01$ cm. The sensitivity analysis is first performed using a small perturbation, say 1% and then using a large perturbation, say 10%. As such, in each case the problem is solved four times for maximizing the heat transfer rate f_1 and minimizing the fin volume f_2. In the first case, the design variable are allowed to vary $\pm 1\%$ from its optimum value, while keeping all other three design variables constant at their optimum values while in the second case the design variable are allowed to vary $\pm 10\%$ from its optimum value. The plots of the deviation of the optimum heat transfer rate f_1^* along the new Pareto front of each case, against the deviation of the corresponding optimum design variable, are shown in Figs. 3.6 and 3.7 respectively.

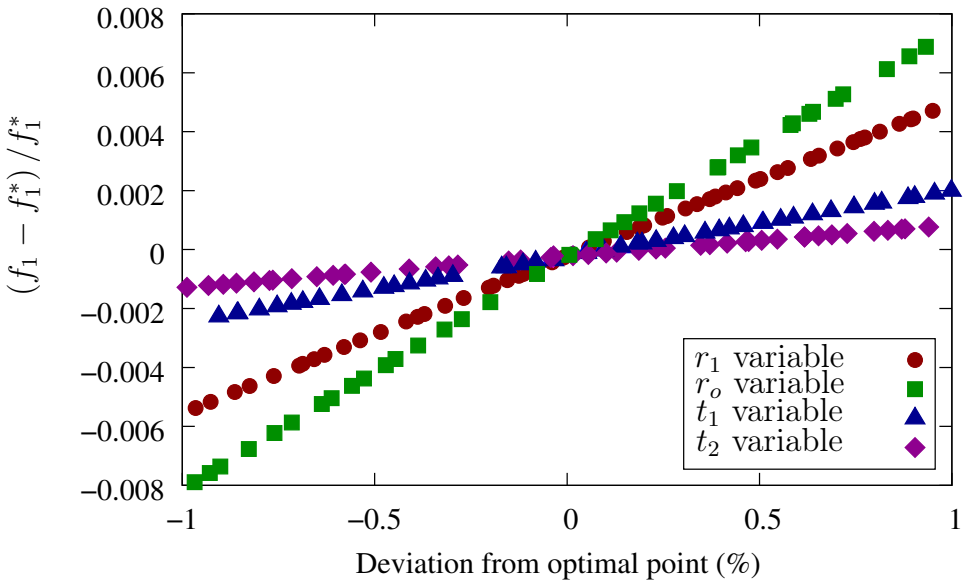

Figure 3.6: Sensitivity analysis of heat transfer rate in terms of design variables using 1% perturbation.

It is found that plots of the deviation of the optimum heat transfer rate f_1^* against the deviation of the corresponding optimum design variable follows the same trends in both the sensitivity analysis using 1% and 10% perturbation. Further it is observed in the plots that the heat transfer rate is more sensitive to the outer radius (r_o) of the fin geometry, followed by that to the fin radius (r_1) at the step change, while the influences of the fin cross-sectional half thicknesses (t_1 and t_2) on the heat transfer rate are comparatively very less. Accordingly, in order to obtain the desired heat

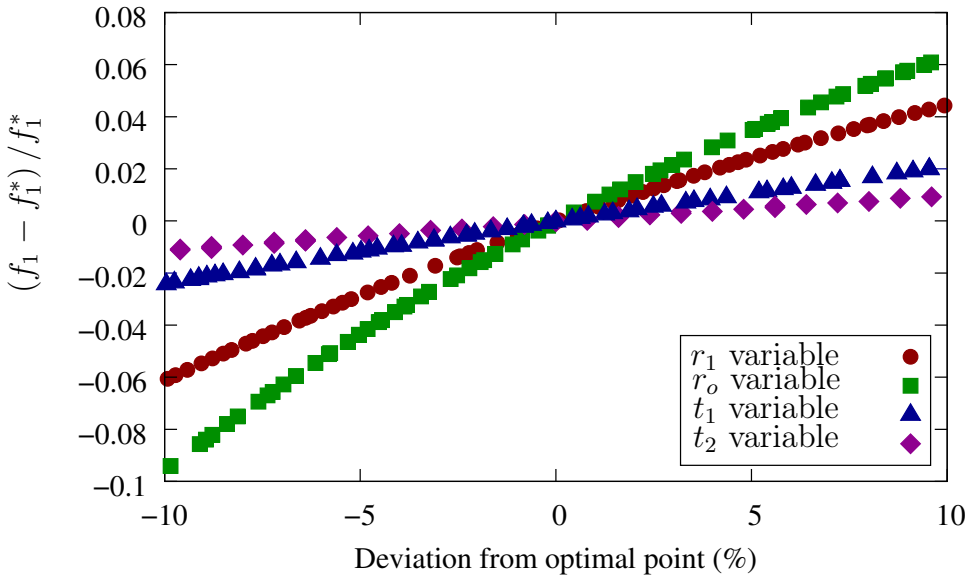

Figure 3.7: Sensitivity analysis of heat transfer rate in terms of design variables using 10% perturbation.

transfer effect, a designer can adjust design variables based upon the availability and practicability of information and resources.

3.2 Fin with linearly varying thickness

The multi-objective optimization of an annular fin of plane profile, attached to a heat exchanger of cylindrical primary surface, is studied here with the assumptions that Poisson's ratio, coefficient of thermal expansion, and modulus of elasticity of the fin material remain constant irrespective of any variation in temperature and the inner and outer radii of the fin are free of traction A schematic diagram of an annular fin of plane profile is shown in Fig. 3.8, where r_b and r_o are respectively the inner and outer radii of the fin, while t represents the cross-sectional half-thickness of the fin with t_b and t_o being its values at the base and tip, respectively. Note that the fin profile will be rectangular if t is constant (i.e., $t_o = t_b$), otherwise it will be taper as shown in Fig. 3.8.

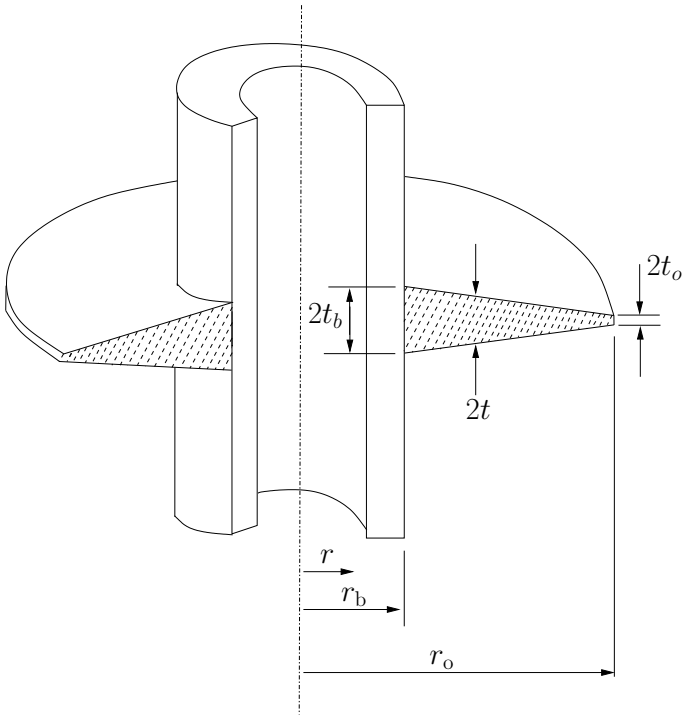

Figure 3.8: Schematic diagram of annular fin of linearly varying thickness.

3.2.1 Formulation for heat transfer equation

Incorporating Eq. (3.1), the one-dimensional steady-state energy balance equation for heat transfer in an axisymmetric thin annular fin can be expressed by Eq. (3.9).

$$\frac{d}{dr}\left[r\left\{1+\beta\left(T-T_\infty\right)\right\}\frac{dT}{dr}\right]+\left[r\left\{1+\beta\left(T-T_\infty\right)\right\}\frac{dT}{dr}\right]\frac{t'}{t} - \frac{hr}{k_a t}\left\{T-T_\infty+\frac{\sigma\epsilon\left(T^4-T_\infty^4\right)}{h}\right\}\left(1+t'^2\right)^{\frac{1}{2}}=0 \quad (3.9)$$

Since it is assumed that temperature at the base of the fin (i.e., T_b) is constant and heat is dissipated from the tip of the fin to the surrounding by convection as well as radiation, Eq. (3.9) is subjected to the boundary conditions given by Eq. (3.10).

$$T = T_b \; ; \qquad \text{at} \quad r = r_b \quad (3.10a)$$

$$-k_a\left\{1+\beta\left(T-T_\infty\right)\right\}\frac{dT}{dr} = h\left(T-T_\infty\right)+\sigma\epsilon\left(T^4-T_\infty^4\right) \; ; \quad \text{at} \quad r = r_o \quad (3.10b)$$

For simplicity of analysis, the fin dimensions and temperature distribution in the fin shown in Fig. 3.8 are non-dimensionalized by defining some dimensionless parameters as given by Eq. (3.11).

$$\left.\begin{array}{lll} X = \frac{r}{r_b} & X_o = \frac{r_o}{r_b} & \zeta = \frac{t_b}{r_b} \\ \delta_d = \beta T_\infty & \gamma_c = \frac{t}{t_b} & Bi = \frac{hr_b}{k_a} \\ \omega = \frac{T}{T_\infty} & \omega_b = \frac{T_b}{T_\infty} & \delta_c = \frac{\beta T_\infty}{(1-\beta T_\infty)} \\ \gamma = \frac{hr_b^2}{t_b k_a (1-\beta T_\infty)} & n_c = \frac{\sigma \epsilon r_b^2 T_\infty^3}{t_b k_a (1-\beta T_\infty)} & m_c = \frac{\sigma \epsilon r_b T_\infty^3}{k_a} \end{array}\right\} \tag{3.11}$$

In terms of the dimensionless parameters defined in Eq. (3.11), the energy balance relation of Eq. (3.9) and its associated boundary conditions of Eq. (3.10) are now expressed in non-dimensional forms as in Eqs. (3.12) and (3.13), respectively.

$$\gamma_c \left\{ (1+\delta_c\omega)\frac{d^2\omega}{dX^2} + (1+\delta_c\omega)\frac{1}{X}\frac{d\omega}{dX} + \delta_c \left(\frac{d\omega}{dX}\right)^2 \right\} + {\gamma_c}'(1+\delta_c\omega)\frac{d\omega}{dX} - \left\{\gamma(\omega-1) + n_c\left(\omega^4-1\right)\right\}\left(1+{\gamma_c}'^2\zeta^2\right)^{\frac{1}{2}} = 0 \tag{3.12}$$

$$\omega = \omega_b; \quad \text{at} \quad X = 1 \tag{3.13a}$$

$$(1-\delta_d+\delta_d\omega)\frac{d\omega}{dX} + Bi(\omega-1) + m_c\left(\omega^4-1\right) = 0; \quad \text{at} \quad X = X_o \tag{3.13b}$$

3.2.2 Formulation of the thermal stress model

Since an annular fin of small thickness can be studied by considering it under the action of an axisymmetric plane stress system [80], the stress-displacement relation-

ships for such an annular fin can be expressed by Eq. (3.14).

$$\sigma_r = \frac{E}{1-\nu^2}\left\{\frac{du}{dr} + \nu\frac{u}{r} - (1+\nu)\alpha_e T\right\} \tag{3.14a}$$

$$\sigma_\theta = \frac{E}{1-\nu^2}\left\{\frac{u}{r} + \nu\frac{du}{dr} - (1+\nu)\alpha_e T\right\} \tag{3.14b}$$

Further, according to the classical theory of elasticity, the equilibrium condition for a fin of plane profile can be expressed in terms of polar coordinates as given by Eq. (3.15).

$$\frac{d\sigma_r}{dr} + \frac{\sigma_r}{t}\frac{dt}{dr} + \frac{\sigma_r - \sigma_\theta}{r} = 0 \tag{3.15}$$

Combining Eqs. (3.14) and (3.15), the equilibrium condition of a fin can be expressed in terms of the displacement field as given by Eq. (3.16).

$$\frac{d^2u}{dr^2} + \left(1 + \frac{rt'}{t}\right)\frac{1}{r}\frac{du}{dr} - \left(1 - \frac{rt'}{t}\nu\right)\frac{u}{r^2} - \left(\frac{dT}{dr} + \frac{t'}{t}T\right)(1+\nu)\alpha_e = 0 \tag{3.16}$$

Since it is assumed in the present study that the outer radius of the annular fin is larger than its thickness, the fin can be studied under a plane stress field, which would cause negligible traction at the end faces (i.e., at the inner and outer radii) [18]. Accordingly, Eq. (3.16) would be subjected to the boundary conditions given by Eq. (3.17).

$$\frac{du}{dr} + \nu\frac{u}{r} - (1+\nu)\alpha_e T_b = 0\ , \quad \text{at} \quad r = r_b \tag{3.17a}$$

$$\frac{du}{dr} + \nu\frac{u}{r} - (1+\nu)\alpha_e T_o = 0\ , \quad \text{at} \quad r = r_o \tag{3.17b}$$

For non-dimensionalizing the thermal stress distribution in the annular fin shown in Fig. 3.8, some dimensionless parameters are defined apart from those in Eq. (3.11).

These new parameters are given Eq. (3.18).

$$\omega_o = \frac{T_o}{T_\infty}, \qquad \psi = \frac{u}{r_o - r_b}, \qquad \eta_c = \frac{r_o - r_b}{r_b} \tag{3.18}$$

In terms of the dimensionless parameters defined in Eqs. (3.11) and (3.18), Eqs. (3.16) and (3.17) are now non-dimensionalized as given by Eqs. (3.19) and (3.20), respectively.

$$\frac{d^2\psi}{dX^2} + \left(1 + \frac{X\gamma_c{}'}{\gamma_c}\right)\frac{1}{X}\frac{d\psi}{dX} - \left(1 - \frac{X\gamma_c{}'}{\gamma_c}\nu\right)\frac{\psi}{X^2} - \frac{(1+\nu)\alpha_e T_\infty}{\eta_c}\left(\omega' + \frac{\gamma_c{}'}{\gamma_c}\omega\right) = 0 \tag{3.19}$$

$$\eta_c\frac{d\psi}{dX} + \eta_c\frac{\nu\psi}{X} - (1+\nu)\alpha_e T_\infty \omega_b = 0\ , \qquad \text{at} \quad X = 1 \tag{3.20a}$$

$$\eta_c\frac{d\psi}{dX} + \eta_c\frac{\nu\psi}{X} - (1+\nu)\alpha_e T_\infty \omega_o = 0, \qquad \text{at} \quad X = X_o \tag{3.20b}$$

3.2.3 Optimization modeling

In the present study the five performance functions, namely heat transfer rate, induced maximum thermal stress, fin volume, fin efficiency, and fin effectiveness, are considered for performance evaluation of the studied annular fin of plane profile.

Further the fin profile shown in Fig. 3.8 is defined by three independent parameters, which are the outer radius (r_o), cross-sectional half thickness at the base (t_b), and cross-sectional half thickness at the outer radius (t_o). It is, therefore, clear that any adjustment in the value of any of these three independent parameters will prompt a new configuration for the annular fin with changed values of the five performance functions.

Accordingly, the fin design problem considered in the present study can be formulated as a multi-objective optimization problem, as given by Eq. (3.21), by

taking the three independent geometric parameters as the design variables and the five performance functions as the objective functions.

$$\left.\begin{array}{rrcl} \text{Determine} & \boldsymbol{x} & \equiv & (r_o, t_b, t_o)^{\mathrm{T}} \\ \text{to maximize} & \boldsymbol{z}(\boldsymbol{x}) & \equiv & \{f_1(\boldsymbol{x}), f_4(\boldsymbol{x}), f_5(\boldsymbol{x})\} \\ \text{minimize} & \boldsymbol{f}(\boldsymbol{x}) & \equiv & \{f_2(\boldsymbol{x}), f_3(\boldsymbol{x})\} \\ \text{subject to} & g_1(\boldsymbol{x}) & \equiv & r_o > r_b \\ & g_2(\boldsymbol{x}) & \equiv & t_o \leq t_b \\ & & & r_o, t_b, t_o \geq 0 \ . \end{array}\right\} \tag{3.21}$$

In Eq. (3.21), constraint $g_1(\boldsymbol{x})$ ensures the existence of the fin, and constraint $g_2(\boldsymbol{x})$ restricts the increase in fin thickness in the outward direction ($t_o = t_b$ will give a rectangular profile, while $t_o < t_b$ will make it taper). Although the last line in Eq. (3.21) ensure just the non-negativity of the design variables as per the requirement of optimization techniques, t_o in practice may be maintained at some specified minimum value in order to avoid any safety hazard resulting from a weak slender tip of the fin. Further, $r_o \ggg 2t_b$ (i.e., the outer radius of the fin is sufficiently larger than its thickness at the base) may be maintained to make the fin thin enough, so that it can be studied under one-dimensional heat conduction in the radial direction only.

The objective functions, $f_1(\boldsymbol{x})$–$f_5(\boldsymbol{x})$ in Eq. (3.21), represent the heat transfer rate, induced maximum thermal stress, fin volume, fin efficiency, and fin effectiveness, respectively. The overall thermal performance of the fin will be enhanced upon maximizing $f_1(\boldsymbol{x})$, $f_4(\boldsymbol{x})$ and $f_5(\boldsymbol{x})$. On the other hand, the minimization of $f_2(\boldsymbol{x})$ and $f_3(\boldsymbol{x})$ will contribute to the enhancement of life expectancy of the fin and reduction in the fin material cost, respectively. In terms of the notations and formulation for heat transfer equation of the fin and thermal stress model as presented in Sections 3.2.1 and 3.2.2 respectively, these objective functions can be formulated

as given by Eq. (3.22).

$$f_1(\boldsymbol{x}) = -kA_b \left.\frac{dT}{dr}\right|_{r=r_b} \tag{3.22a}$$

$$f_2(\boldsymbol{x}) = \left[\left(\sigma_r^2 - \sigma_r\sigma_\theta + \sigma_\theta^2\right)^{\frac{1}{2}}\right]_{\max} \tag{3.22b}$$

$$f_3(\boldsymbol{x}) = V \tag{3.22c}$$

$$f_4(\boldsymbol{x}) = \frac{f_1(\boldsymbol{x})}{hA_s\left(T_b - T_\infty\right) + \sigma\epsilon A_s\left(T_b^4 - T_\infty^4\right)} \tag{3.22d}$$

$$f_5(\boldsymbol{x}) = \frac{f_1(\boldsymbol{x})}{hA_b\left(T_b - T_\infty\right) + \sigma\epsilon A_b\left(T_b^4 - T_\infty^4\right)} \tag{3.22e}$$

where, $A_b = 4\pi r_b t_b$

Using the Simpson's $\frac{1}{3}$ rule for numerical integration, the fin volume V in Eq. (3.22c) is evaluated as given by Eq. (3.23).

$$V = \frac{4}{3}\pi \sum_{n=2,4,\ldots}^{N} r_{n-1}\left(r_n - r_{n-1}\right)\left(t_{n-2} + 4\ t_{n-1} + t_n\right) \tag{3.23}$$

Further, the heat transfer surface area A_s in Eq. (3.22d) is evaluated from the fin geometry as expressed by Eq. (3.24).

$$A_s = 4\pi r_o t_o + 2\pi \sum_{n=1}^{N}\left(r_n + r_{n-1}\right)\left\{\left(r_n - r_{n-1}\right)^2 + \left(t_{n-1} - t_n\right)^2\right\}^{\frac{1}{2}} \tag{3.24}$$

3.2.4 Solution procedure

The non-dominated sorting genetic algorithm II (NSGA-II) is employed to solve the fin design problem formulated in Eq. (3.21) as a multi-objective optimization model. The working steps of (NSGA-II) in the context of the present study is summarized in Section A.2.4.

The heat transfer rate $f_1(\boldsymbol{x})$ given by Eq. (3.22a) is computed numerically by

solving the problem governing Eq. (3.12) along with its associated boundary conditions in Eq. (3.13). Similarly, the problem governing Eq. (3.19) along with its associated boundary conditions in Eq. (3.20) is solved to compute the induced maximum thermal stress $f_2(\boldsymbol{x})$ given by Eq. (3.22b). For these, the sets of Eqs. (3.12) and (3.13), and Eqs. (3.19) and (3.20) are solved first by employing the hybrid spline difference method (HSDM) so as to evaluate the dimensionless temperature field (ω) and displacement field (ψ), respectively. The discrete relationships used in HSDM can be expressed as Eq. (A.9).

To assess the correctness of the algorithm for solving the direct problem, the results of HSDM for temperature and stress fields are compared with those of Mallick et al. [63]. The comparison is shown in Fig. 3.9, where it is found that the numer-

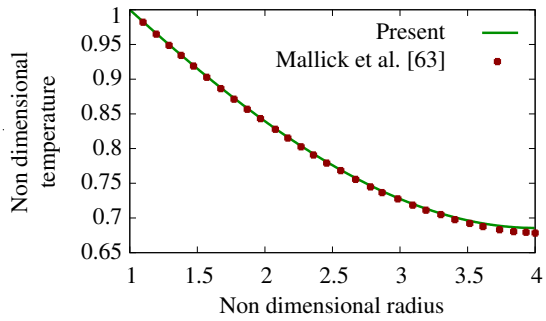

(a) Temperature distribution.

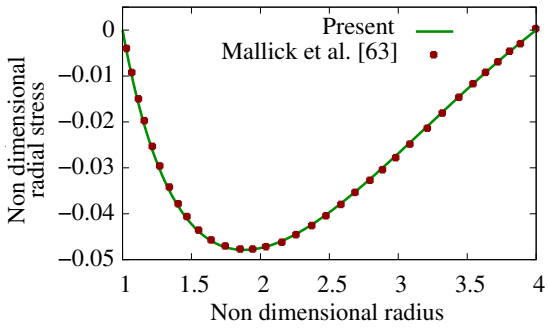

(b) Radial stress distribution.

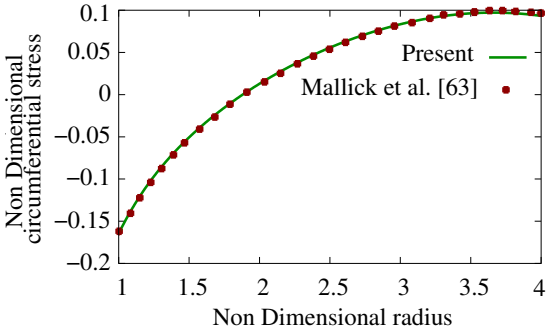

(c) Circumferential stress distribution.

Figure 3.9: Comparison of temperature and stress distribution with those of Mallick et al. [63].

ical results of HSDM reveal a very good agreement with the deterministic results reported by Mallick et al. [63], thus illustrating the correctness of the algorithm used for solving the direct problem. For clarity of the comparison, the results shown in Fig. 3.9 take into account the same parameter values and similar boundary condi-

tions.

The detail procedure for evaluating $f_1(\boldsymbol{x})$ and $f_2(\boldsymbol{x})$ in Step (3) of NSGA-II, through the HSDM scheme expressed by Eq. (A.9), is as follows:

(a) Discretize Eqs. (3.12) and (3.13) as in Eq. (A.9).

(b) Evaluate p_n $(n = 0, 1, \ldots, N)$ by solving the discretized form of Eqs. (3.12) and (3.13) using the variant of the Thomas algorithm proposed by Martin and Boyd [64].

(c) At all the grid points, evaluate the dimensionless temperature distribution and their derivatives up to the second order, i.e., ω_n, ω'_n and ω''_n using the values of p_n in Eq. (A.9).

(d) Evaluate the temperature gradient at the base of the fin, i.e., $\frac{dT}{dr}\big|_{r=r_b}$, from the dimensionless temperature gradient ω'_0 at the base of the fin.

(e) Evaluate $f_1(\boldsymbol{x})$ using the value of $\frac{dT}{dr}\big|_{r=r_b}$ in Eq. (3.22a).

(f) Repeat Steps (a) and (b) for Eqs. (3.19) and (3.20), and then evaluate the dimensionless displacement and their derivatives up to the second order (i.e., ψ_n, ψ'_n and ψ''_n) using the values of p_n in Eq. (A.9).

(g) Evaluate the displacement field, along with their first order gradient, using the values of ψ_n and ψ'_n throughout the fin length in the radial direction.

(h) Evaluate the radial and circumferential thermal stresses (i.e., σ_r and σ_θ, respectively) throughout the fin length using the temperature distribution, and displacement field and its first order derivative in Eq. (3.14).

(i) Evaluate the resultant thermal stress throughout the fin length, and then find its maximum value as $f_2(\boldsymbol{x})$ expressed by Eq. (3.22b).

3.2.5 Numerical experimentation and discussion

In the present study, an annular fin consisting of plane surfaces is studied in a convective and radiative environment with constant base temperature and variable thermal conductivity. For numerical experimentation, the considered operating conditions and thermal properties of the fin material along with the fin geometry with reference to Fig. 3.8 are given in Table 3.4, while the user-defined algorithmic parameter settings for NSGA-II are given in Table 3.3. After fixing the sets of input parameters, the fin size optimization problem as formulated in Eq. (3.21) is investigated under two scenarios of the considered five objective functions $f_1(\boldsymbol{x})$–$f_5(\boldsymbol{x})$ given by Eq. (3.22). The objective functions are optimized in different pairs in the first scenario, while all of them are optimized simultaneously in the second scenario.

Table 3.4: Operating conditions, fin material properties, and fin geometry for linearly varying thickness annular fin.

Parameter	Value/ range of value
Ambient temperature, T_∞	300 K
Temperature of the fin at the base, T_b	600 K
Convective heat transfer coefficient on the fin surface, h	50 W/m^{2}K
Thermal conductivity of the fin material at T_∞, k_a	186 W/mK
Parameter for variable thermal conductivity, β	-0.00018 K^{-1}
Emissivity of the fin material, ϵ	0.8
Base radius of the fin, r_b	2.0 cm
Outer radius of the fin, r_o	3.5–15.0 cm
Half thickness of the fin at the base, t_b and tip, t_o	0.01–0.3 cm

3.2.5.1 Scenario I

The heat transfer rate (f_1) and the maximum thermal stress (f_2) are assumed as the two primary objective functions to be optimized in the fin design problem at hand (f_1 is to be maximized and f_2 is to be minimized). For further assessment, the fin design is studied in the second step maximizing the heat transfer rate (f_1) separately with minimizing the fin volume (f_3), maximizing the fin efficiency (f_4) and maximizing the fin effectiveness (f_5). The obtained respective final Pareto fronts are shown in Figs. 3.10(a)–3.10(d). The solutions of the Pareto front in Fig. 3.10(a) depict the trade-off (conflicting) nature between the heat transfer rate and thermal stress.

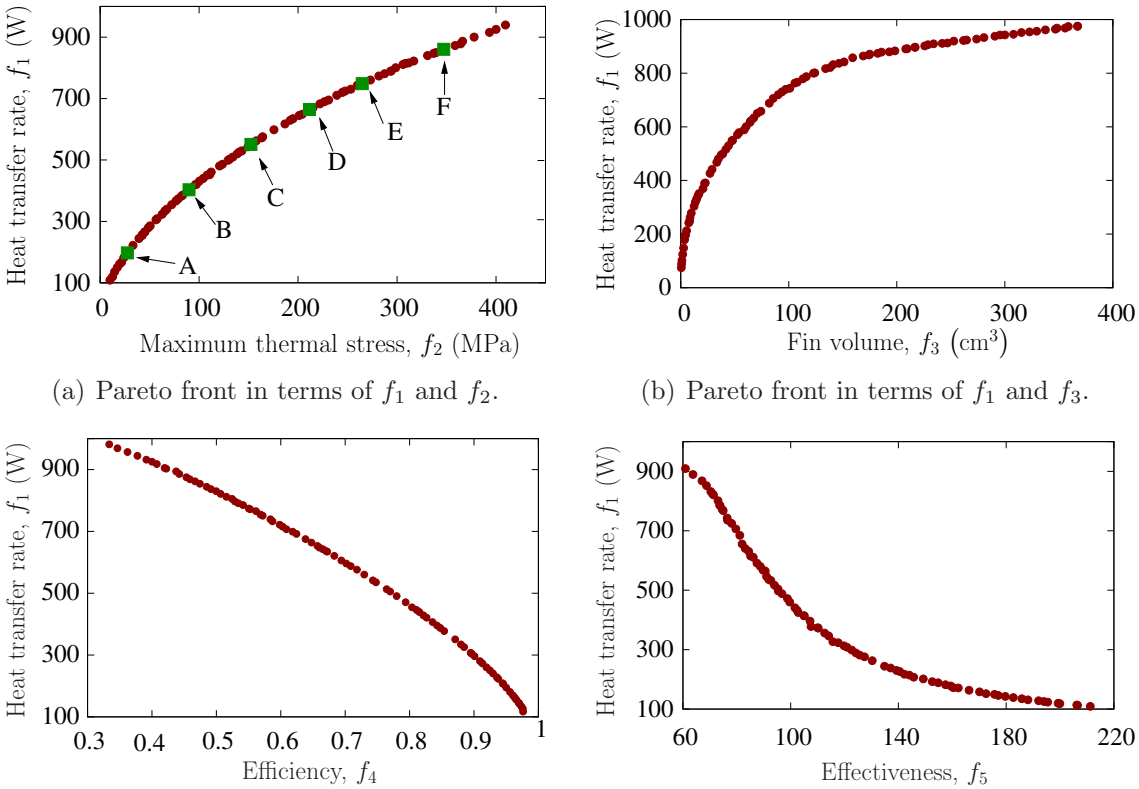

(a) Pareto front in terms of f_1 and f_2.

(b) Pareto front in terms of f_1 and f_3.

(c) Pareto front in terms of f_1 and f_4.

(d) Pareto front in terms of f_1 and f_5.

Figure 3.10: Pareto fronts for pairwise objective functions of linearly varying thickness fin.

Similar conflicting nature of the heat transfer rate with fin volume, fin efficiency and fin effectiveness are also seen in Figs. 3.10(b)–3.10(d), respectively.

Six selective efficient fin geometries, corresponding to trade-off solutions A–F of Fig. 3.10(a), are shown in Fig. 3.11, where the variations in the patterns of the fin profiles are noticeable. Calculating the values of f_3–f_5 for these fin configurations, which are also shown in Fig. 3.11 along with the optimized values of f_1 and f_2, it is observed in these particular six profiles that with increasing f_1 and f_2, f_3 and f_5 also increase continuously, while f_4 decreases.

3.2.5.2 Scenario II

Optimizing the objective functions of the annular fin design problem in pairs, it is observed in Section 3.2.5.1 that the heat transfer rate varies differently with different

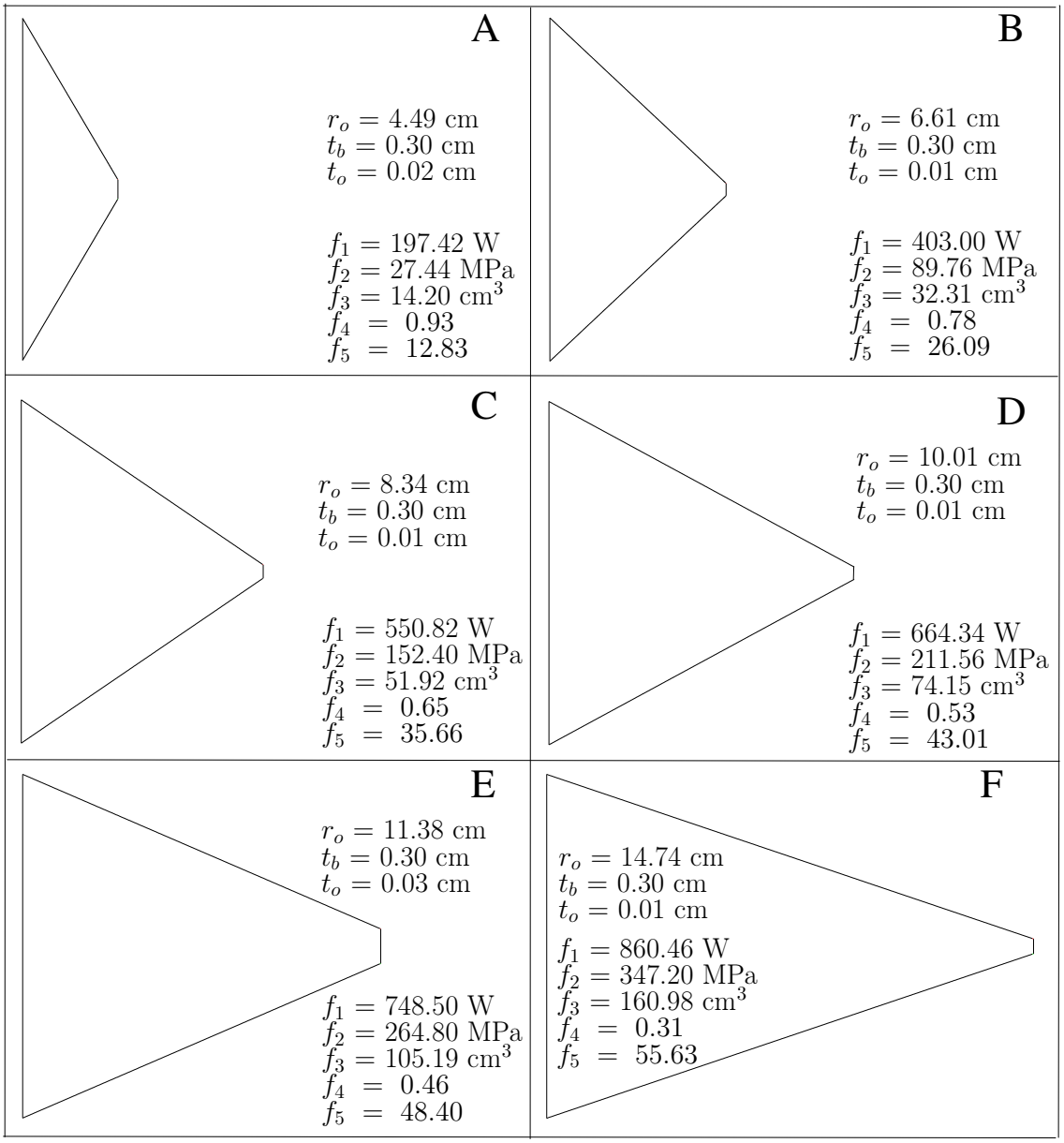

Figure 3.11: Selective geometries of linearly varying thickness fin (corresponding to trade-off solutions A–F of Fig. 3.10(a). In these plots, the scale along the axial (vertical) direction is 15 times larger than that along the radial (horizontal) direction.)

objective functions without any common pattern. Therefore, all the considered five objective functions, i.e.,f_1–f_5 given by Eq. (3.22), are next optimized simultaneously with the expectation for arriving at a general conclusion.

The obtained five-dimensional Pareto front is plotted in a parallel coordinate system as shown in Fig. 3.12, which clearly depicts the conflicting nature of various objective functions. For instance, the solution of the Pareto front having maximum heat transfer rate exhibit a very high fin volume, a reasonably high maximum ther-

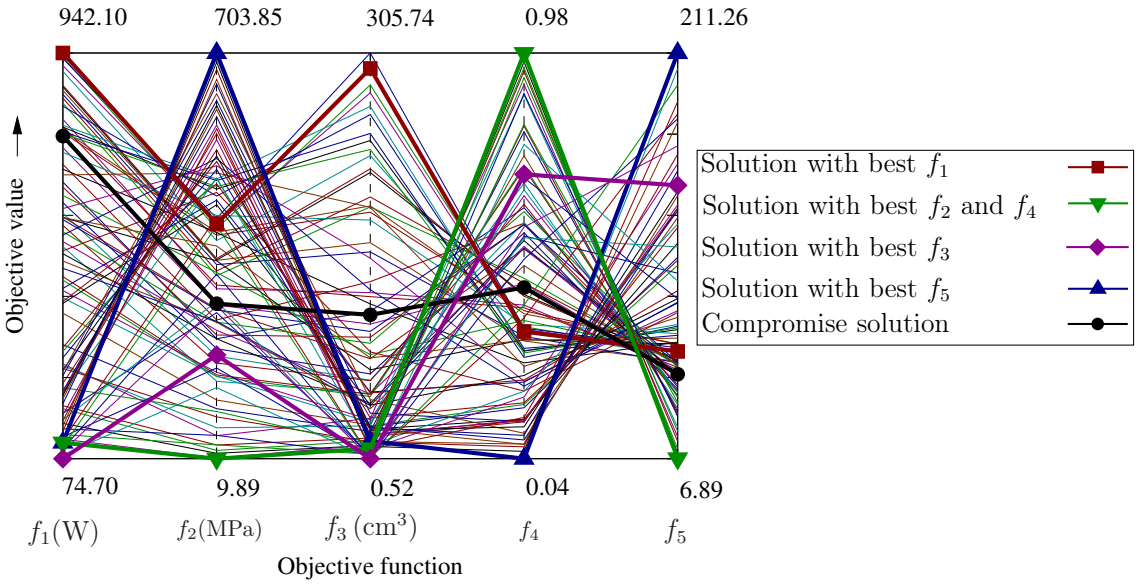

Figure 3.12: Five-dimensional Pareto front in a parallel coordinate system.

mal stress, while a reasonably low fin efficiency and fin effectiveness. The degree of zigzagness of the various cross lines demonstrates the trade-off sharpness of the objective values between various efficient solutions. It is also to be noted that a very high value of thermal stress in developed in the fin at extremely low value of fin volume. It is now up to a designer to adopt a balanced solution based upon the availability and practicability of information and resources for the problem at hand. Such a compromised solution, bearing some intermediate values of the objective functions, is also shown in Fig. 3.12 by a thick crossed line.

3.2.6 Sensitivity analysis

Finally, in order to investigate the effect of each design variable on the heat transfer rate and maximum thermal stress developed in the fin, a sensitivity analysis is performed. For this purpose, the design variables are allowed to vary ±40% from a chosen particular point in the design space ($t_b^\dagger = 0.20$ cm, $t_o^\dagger = 0.10$ cm and $r_o^\dagger = 9.25$ cm). The corresponding heat transfer rate $f_1^\dagger$ and the maximum thermal stress developed $f_2^\dagger$ for the chosen point are 573.51 W and 268.24 MPa, respectively. In this analysis, the problem is solved three times, each time allowing a design variable to vary from its chosen value, while keeping the other two

design variables fixed. The plots of the deviation of the heat transfer rate and the maximum thermal stress developed against the characteristic variation of the corresponding design variables, are shown in Fig. 3.13(a) and Fig. 3.13(b), respectively.

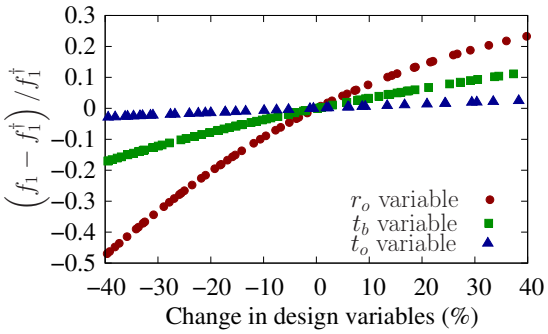

(a) Variation of the heat transfer rate with the design variables.

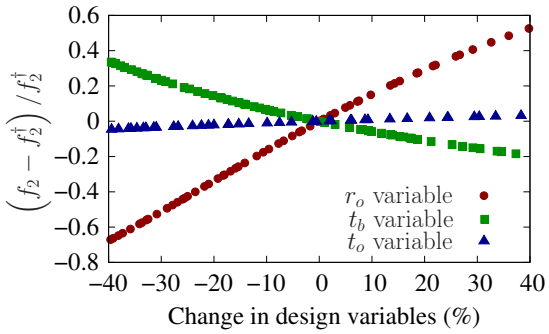

(b) Variation of the maximum thermal stress with the design variables.

Figure 3.13: Sensitivity analysis of heat transfer rate and maximum thermal stress in terms of design variables.

It is observed in the plots that both the heat transfer rate and maximum thermal stress developed are more sensitive to the outer radius (r_o) of the fin, followed by that to the fin cross-sectional half thickness at the base (t_b), while the influences of the fin cross-sectional half thickness at the outer radius (t_o) are comparatively very less in both the cases. Accordingly, in order to acquire the desired heat transfer effect maintaining the maximum thermal stress, a designer will have the freedom to choose economic combinations of the design variables based upon the accessibility and practicability of information and resources. It may be noticed in Fig. 3.13 that, with an increase in t_b, the heat transfer rate in the fin increases and the induced maximum thermal stress decreases. Since problem related all other parameter values were kept constant, this happened because of the fact that an increase in t_b decreases the conductive resistance to heat flow, thus increasing the heat transfer rate. Further increased heat transfer rate results in a more uniform temperature distribution along the radial direction of the fin, which lead to decreasing thermal stress in the fin.

3.3 Fin of non-linearly varying thickness

The problem in the present study is a non-linearly varying thickness annular fin attached to a heat exchanger of cylindrical primary surface. The Poisson's ratio, modulus of elasticity and coefficient of thermal expansion of the fin material are assumed to remain constant with temperature. A schematic diagram of a non-linearly varying thickness annular fin is shown in Fig. 3.14. The inner and outer

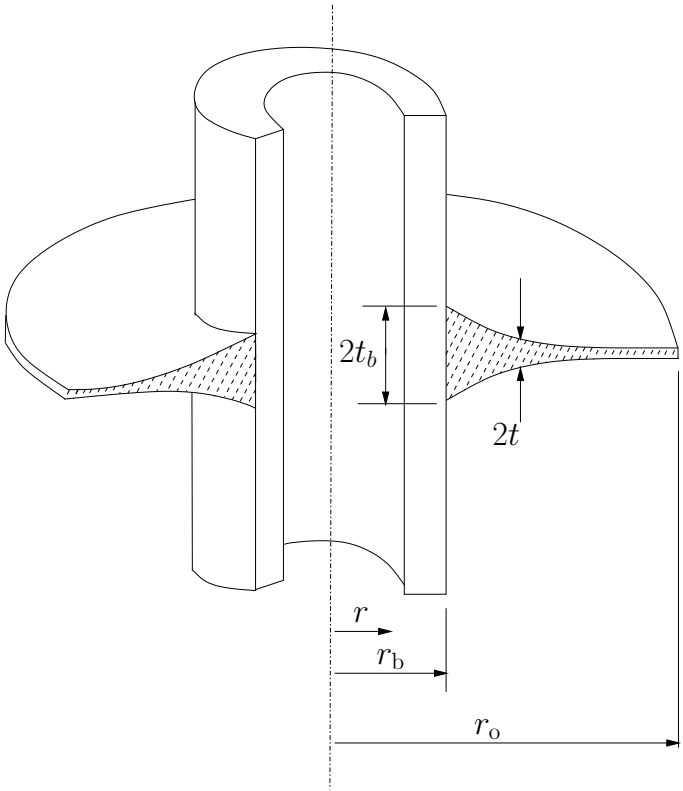

Figure 3.14: Schematic diagram of non-linearly varying thickness annular fin.

radii of the fin are r_b and r_o respectively. The cross-sectional half-thickness of the fin is t with t_b being that at the base of the fin.

3.3.1 Formulation for heat transfer equation

The formulation for heat transfer equation of non-linearly varying thickness annular fin is similar to that of linearly varying thickness annular fin profile as given in Section 3.2.1.

3.3.2 Formulation of the thermal stress model

The formulation for the thermal stress model of non-linearly varying thickness annular fin is similar to that of linearly varying thickness annular fin as given in Section 3.2.2.

3.3.3 Optimization modeling

In the present study the performance of the studied non-linearly varying thickness annular fin will be evaluated in different combinations of five performance functions, which are heat transfer rate, maximum thermal stress induced in the fin, fin volume, fin efficiency, and fin effectiveness. Further the profile of the fin, as shown in Fig. 3.14, can be defined in terms of m number of control points of a B-spline curve. Therefore, it is clear that a change in any of these control points will lead to a new design of the annular fin with different values of the five performance functions.

In the optimization process, the optimum shape of the fin profile can be obtained by finding the optimum values of the control points, which are regarded as unknowns. The first control point is positioned at the base of the fin that can move freely along the y-axis, so that its x-value will represent the predefined fixed radius at the base of the fin while its y-value will represent the half thickness of the fin at the base. The last control point can move freely in the xy-plane, representing the length of the fin by its x-value and the half thickness of the fin at the tip by its y-value. The intermediate control points can also move in the xy-plane with fixed or increasing x-values and decreasing y-values in between those of the first and last control points. Accordingly, treating the m number of control points as the design variables and the five performance functions as the objective functions to be optimized simultaneously, the considered fin design problem can be formulated as a

multi-objective optimization problem as given by Eq. (3.25).

$$\left.\begin{array}{rrcl} \text{Determine} & \boldsymbol{x} & \equiv & (P_1, P_2, P_3, \cdots\cdots, P_m)^{\mathrm{T}} \\ \text{to maximize} & \boldsymbol{z}(\boldsymbol{x}) & \equiv & \{f_1(\boldsymbol{x}), f_4(\boldsymbol{x}), f_5(\boldsymbol{x})\} \\ \text{minimize} & \boldsymbol{f}(\boldsymbol{x}) & \equiv & \{f_2(\boldsymbol{x}), f_3(\boldsymbol{x})\} \\ \text{subject to} & g_1(\boldsymbol{x}) & \equiv & x_1 < x_2 \leq \cdots \leq x_m \\ & g_2(\boldsymbol{x}) & \equiv & y_1 \geq y_2 \geq \cdots \geq y_m \end{array}\right\} \tag{3.25}$$

In Eq. (3.25), $P_i = (x_i, y_i)$ is the ith control point and m is the total number of control points of the B-spline curve representing the fin profile, while $x_1 = r_b$, $y_1 = t_b$, $x_m = r_o$ and $y_m = t_o$ as considered in Fig. 3.14. The constraints $g_1(\boldsymbol{x})$ and $g_2(\boldsymbol{x})$ in Eq. (3.25) make the control points distributed along the radially outward direction of the fin with non-increasing values in the direction of the fin thickness. In other words, $g_1(\boldsymbol{x})$ and $g_2(\boldsymbol{x})$ resists the control points to form an unphysical shape of the B-spline curve, so as to give a viable fin profile. Further, in order to represent a practical scenario, a sharp outer edge of the fin may be avoided by fixing $y_m > 0$.

The five objective functions, represented by $f_1(\boldsymbol{x})$–$f_5(\boldsymbol{x})$ in Eq. (3.25), are the heat transfer rate, maximum thermal stress developed, fin volume, fin efficiency, and fin effectiveness, respectively. The maximization of $f_1(\boldsymbol{x})$, $f_4(\boldsymbol{x})$ and $f_5(\boldsymbol{x})$ enhances the overall thermal performance of the fin, while the minimization of $f_2(\boldsymbol{x})$ increases its life expectancy and minimization of $f_3(\boldsymbol{x})$ reduces the fin material cost. These objective functions, in terms of the notations and formulation for heat transfer equation and thermal stress model of the fin as presented in Sections 3.3.1 and 3.3.2 respectively, are similar to that of linearly varying thickness fin as expressed by Eq. (3.22).

3.3.4 Solution procedure

The solution procedure of non-linearly varying thickness annular fin is similar to that of linearly varying thickness annular fin as given in Section 3.2.4.

3.3.5 Numerical experimentation and discussion

The rate of convergence of an optimization process is dependent on the number of design variables also, among others. It usually decreases with increasing number of design variables. Since in terms of flexibility and stiffness, cubic curves with open uniform knot vector and of order 4 are considered to be sufficient in most of the engineering analysis, the same is considered for the B-spline curve representing the fin profile investigated in this work. Further, since the number of control points of a B-spline curve must be more than the chosen polynomial degree by at least two units in order to have a local control on the curve [75], five control points are considered here to approximate the fin profile. The coordinates of these five control points of the B-spline curve are treated here as the design variables of the studied fin design problem.

In the present study, the non-linearly varying thickness annular fin is analyzed in a convective and radiative environment with a constant temperature at the base of the fin and variable thermal conductivity for the fin material. The considered operating conditions and thermal properties of the fin material along with fin geometry are listed in Table 3.5 with reference to Fig. 3.14, and the user-defined algorithmic parameter settings for NSGA-II are given in Table 3.3. With the above sets of input parameters and randomly generated NSGA-II population, the fin configuration optimization problem formulated in Eq. (3.25) is analyzed under two scenarios of the considered five objective functions f_1–f_5 given by Eq. (3.22). In the first scenario, the objective functions are optimized in various pairs, while in the second scenario all of them are optimized simultaneously.

Table 3.5: Operating conditions, fin material properties, and fin geometry for non-linearly varying thickness annular fin.

Parameter	Value/ range of value
Ambient temperature, T_∞	300 K
Temperature of the fin at the base, T_b	600 K
Convective heat transfer coefficient on the fin surface, h	50 W/m^{2}K
Thermal conductivity of the fin material at T_∞, k_a	186 W/mK
Parameter for variable thermal conductivity, β	-0.00018 K^{-1}
Emissivity of the fin material, ϵ	0.8
Base radius, r_b	2.0 cm
Outer radius, r_o	3.5–15.0 cm
Half thickness of the fin, t	0.01–0.3 cm

3.3.5.1 Scenario I

Initially the fin design optimization problem is analyzed for maximization of the heat transfer rate (f_1) and minimization of the maximum thermal stress (f_2) developed in the fin. The obtained final Pareto front, shown in Fig. 3.15(a), contains a

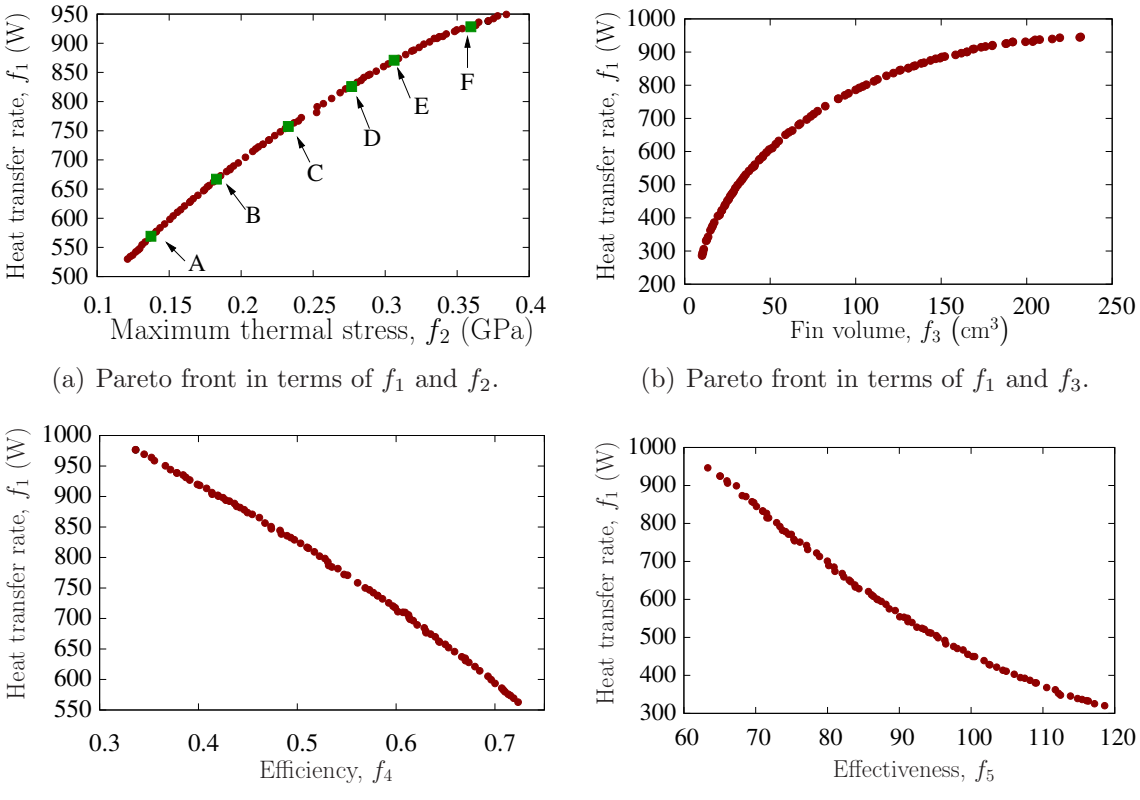

(a) Pareto front in terms of f_1 and f_2.

(b) Pareto front in terms of f_1 and f_3.

(c) Pareto front in terms of f_1 and f_4.

(d) Pareto front in terms of f_1 and f_5.

Figure 3.15: Pareto fronts for pairwise objective functions of non-linearly varying thickness fin.

set of trade-off solutions in terms of f_1 and f_2, which clearly exhibits the conflicting nature between the heat transfer rate and the maximum thermal stress. Six num-

ber of selective efficient fin geometries, corresponding to trade-off solutions A–F of Fig. 3.15(a), are shown in Fig. 3.16, where the patterns of variation in the fin pro-

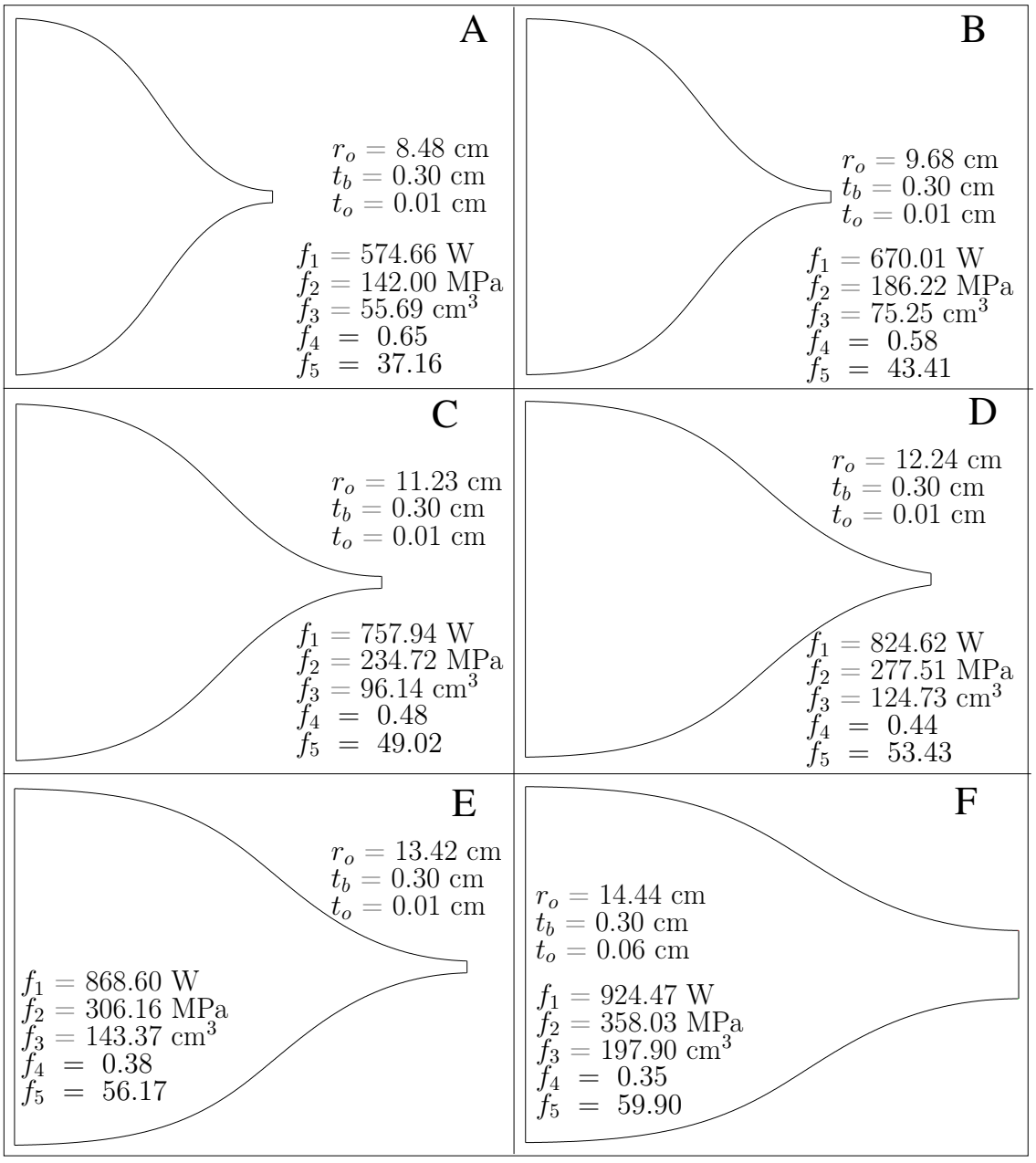

Figure 3.16: Selective efficient fin configurations (corresponding to trade-off solutions A–F of Fig. 3.15(a). In these plots, the scale along the axial (vertical) direction is fifteen times larger than that along the radial (horizontal) direction.)

files are noticeable. For these fin configurations, the values of other three objective functions, f_3–f_5, are also evaluated and shown in Fig. 3.16, where it is observed that with respect to increasing f_1 and f_2, f_3 and f_5 also increase continuously, but f_4 shows the reverse trend.

In view of above, the fin configuration optimization problem is analyzed in the second step for maximization of f_1 separately with minimization of f_3, maximization of f_4, and maximization of f_5. The obtained final Pareto fronts of these three cases are shown in Figs. 3.15(b)–3.15(d), respectively. The Pareto front in Fig. 3.15(b) shows the conflicting nature of heat transfer rate with fin volume, i.e., with improvement in f_1, f_3 degrades by some amount, and *vice-versa*. Next analyzing the Pareto fronts in Figs. 3.15(c) and 3.15(d), it is observed that the heat transfer rate conflicts with both fin efficiency and fin effectiveness, i.e., a higher value of f_1 reduces both f_4 and f_5.

3.3.5.2 Scenario II

Analyzing the objective functions in pairs, it is observed in the Section 3.3.5.1 that the variations of heat transfer rate with other objective functions are different, leading to no common pattern. Therefore, in order to arrive at a general scenario, all the five considered objective functions, i.e., f_1–f_5 given by Eq. (3.22), are optimized simultaneously. The obtained five-dimensional Pareto front is plotted in a parallel coordinate system as shown in Fig. 3.17 in which the conflicting nature of different

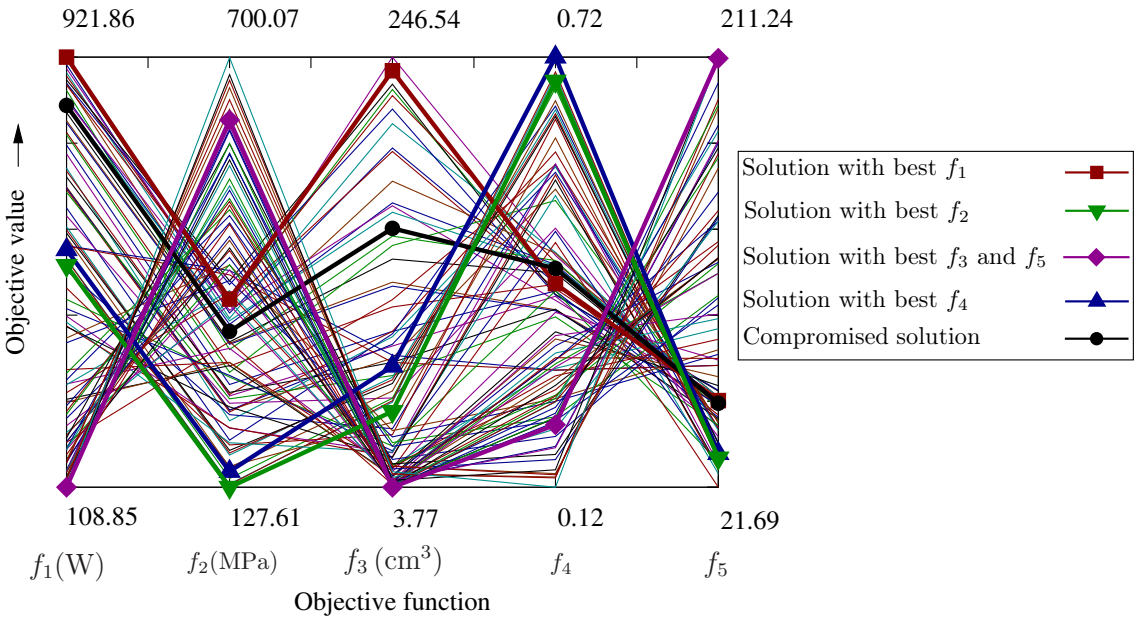

Figure 3.17: Five-dimensional Pareto front in two-dimensional parallel coordinate system.

objective functions can be noticed clearly. For example, the solution corresponding to the maximum heat transfer rate bears a moderately high thermal stress and fin efficiency, and a very high fin volume, while a low fin effectiveness. It is also to be noted that at an extremely low value of fin volume, a very high thermal stress is developed in the fin. Based upon the availability and practicability of information and resources for the problem at hand, a designer can now enjoy the flexibility to adopt a balanced solution out of multiple alternatives provided by the Pareto front. One such compromised solution, which bears some intermediate values of the objective functions, is also shown in Fig. 3.17 by a thick crossed line.

3.4 Comparison of different fins

The problem in the present study is an annular fin of various profiles (namely step change in thickness, non-linearly varying thickness, and uniform thickness) attached to a heat exchanger of cylindrical primary surface. Fig. 3.18 shows the schematic

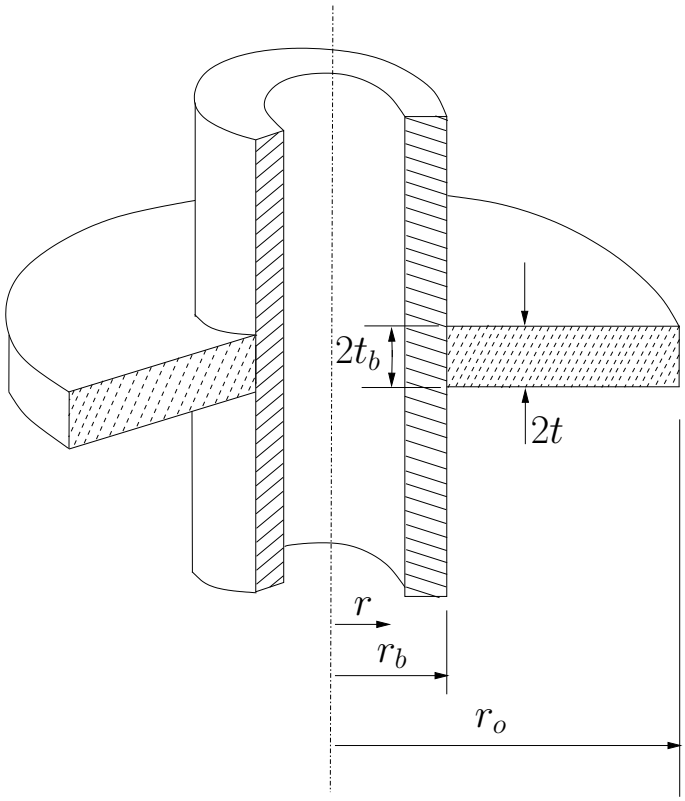

Figure 3.18: Schematic diagram of annular fins of uniform thickness.

diagram of annular fins of uniform thickness whereas fin of step change in thickness and non-linearly varying thickness are already shown in Figs. 3.1 and 3.14 respectively. Here r is the radial distance with r_b and r_o respectively as its radial values at the inner and outer surfaces of each fin, $t(= t_b = t_o)$ represents the cross-sectional half-thickness of the uniform thickness fins.

3.4.1 Common formulation for heat transfer equation

The formulation for heat transfer equation of stepped fin and non-linearly varying thickness fin is already discussed in Section 3.1.1 and Section 3.3.1 respectively. For uniform thickness fin profile, $t' = 0$ in Eq. (3.9).

3.4.2 Common optimization modeling

In the present study the performance of the studied annular fin of various profiles are evaluated in different combinations of three performance functions, which are heat transfer rate, fin volume and fin efficiency. Accordingly, the multi-objective optimization problem is formulated here in a general form for maximizing the heat transfer rate ($f_1(\boldsymbol{x})$) and fin efficiency ($f_3(\boldsymbol{x})$) and minimizing the fin volume ($f_2(\boldsymbol{x})$).

3.4.2.1 Stepped fin

The geometry of the step fin, as shown in Fig. 3.1, is defined in terms of four parameters, which are radius of the fin at the point of step change in thickness (r_1), outer radius of the fin (r_o), cross-sectional half thickness of the thick (first) step of the fin (t_1), and cross-sectional half thickness of the thin (second) step of the fin (t_2). Taking these four parameters as the variables, the design of the step fin can be formulated as a multi-objective optimization problem as given by Eq. (3.26).

$$\left.\begin{array}{rrcl} \text{Determine} & \boldsymbol{x} & \equiv & (r_1, r_o, t_1, t_2)^{\mathrm{T}} \\ \text{to maximize} & \boldsymbol{z}(\boldsymbol{x}) & \equiv & \{f_1(\boldsymbol{x}), f_3(\boldsymbol{x})\} \\ \text{minimize} & \boldsymbol{f}(\boldsymbol{x}) & \equiv & \{f_2(\boldsymbol{x})\} \\ \text{subject to} & g_1(\boldsymbol{x}) & \equiv & r_1 > r_b \\ & g_2(\boldsymbol{x}) & \equiv & r_o > r_1 \\ & g_3(\boldsymbol{x}) & \equiv & t_1 > t_2 \\ & & & r_1, r_o, t_1, t_2 \geq 0 \ . \end{array}\right\} \tag{3.26}$$

In Eq. (3.26), the existence of two steps in the fin is ensured by constraints $g_1(\boldsymbol{x})$ and $g_2(\boldsymbol{x})$, while two different cross-sectional thicknesses of the two steps are ensured by constraint $g_3(\boldsymbol{x})$. The last line in Eq. (3.26) makes the design variables non-negative.

3.4.2.2 Non-linearly varying and uniform thickness fins

The profile of the non-linearly varying thickness fin as shown in Fig. 3.14 is represented by a B-spline curve, which is defined by some control points. Hence, m number of such control points, $P_i(x_i, y_i)$ ($i = 1$ to m), are taken as the design variables, whose x values will represent the radial distances starting from the base of the fin and associated y values will define the half-thickness of the fin falling on the B-spline curve. On the other hand, the profile of the uniform thickness fin, as shown in Fig. 3.18, is defined by a single point $P_1 = (x, y)$, whose x and y values will give respectively the outer radius and half-thickness of the fin. Accordingly, the optimization problem for both the profiles can be formulated jointly as given by Eq. (3.27).

$$\left.\begin{array}{rrcl} \text{Determine} & \boldsymbol{x} & \equiv & \{P_i | P_i \ ; \ i = 1 \text{ to } m\} \\ \text{to maximize} & \boldsymbol{z}(\boldsymbol{x}) & \equiv & \{f_1(\boldsymbol{x}), f_3(\boldsymbol{x})\} \\ \text{minimize} & \boldsymbol{f}(\boldsymbol{x}) & \equiv & \{f_2(\boldsymbol{x})\} \\ \text{subject to} & g_1(\boldsymbol{x}) & \equiv & x_1 < x_2 \leq \cdots \leq x_m \\ & g_2(\boldsymbol{x}) & \equiv & y_1 \geq y_2 \geq \cdots \geq y_m \end{array}\right\} \tag{3.27}$$

In the case of the non-linearly varying thickness fin, $P_i = (x_i, y_i)$ in Eq. (3.27) is the ith control point of the B-spline curve representing the fin profile and m is the total number of control points. According to the notations used in Fig. 3.14, $x_1 = r_b$, $y_1 = t_b$, $x_m = r_o$ and $y_m = t_o$. Constraints $g_1(\boldsymbol{x})$ and $g_2(\boldsymbol{x})$ in Eq. (3.27) ensure that the control points are distributed along the radially outward direction of the fin with non-increasing values in the direction of the fin thickness, so as to avoid any unpleasant fin profile. Further, $y_m > 0$ can be set in order to represent a practical scenario by avoiding a sharp outer edge of the fin.

In Eq. (3.27), $m = 1$ for uniform thickness fin, indicating a single design point as stated above. Further, constraints $g_1(\boldsymbol{x})$ and $g_2(\boldsymbol{x})$ are not applicable in this case.

3.4.2.3 Formulation of objective functions

The three objective functions, $f_1(\boldsymbol{x})$–$f_3(\boldsymbol{x})$ expressed in Eqs. (3.26) and (3.27), are the heat transfer rate, fin volume, and fin efficiency, respectively. The maximization of $f_1(\boldsymbol{x})$ and $f_3(\boldsymbol{x})$ enhances the overall thermal performance of the fin, while the minimization of $f_2(\boldsymbol{x})$ reduces the fin material cost. In terms of the notations and formulations for heat transfer equation of the fins as presented in Section 3.4.1, these can be given by Eq. (3.28).

$$f_1(\boldsymbol{x}) = -kA_b \left.\frac{dT_i}{dr}\right|_{r=r_b} \tag{3.28a}$$

$$f_2(\boldsymbol{x}) = V \tag{3.28b}$$

$$f_3(\boldsymbol{x}) = \frac{f_1(\boldsymbol{x})}{hA_s\left(T_b - T_\infty\right) + \sigma\epsilon A_s\left(T_b^4 - T_\infty^4\right)} \tag{3.28c}$$

$$\text{where,} \quad A_b = \begin{cases} 4\pi r_b t_1 \ ; \ \text{for step fin.} \\ 4\pi r_b t_b \ ; \ \text{for uniform/non-linearly varying thickness fins} \end{cases}$$

In Eq. (3.28a), A_b is the base area of the fin. The fin volume V, appearing in

Eq. (3.28b), is expressed by Eq. (3.29).

$$V = \begin{cases} 2\pi \left\{ t_1 \left(r_1^2 - r_b^2 \right) + t_2 \left(r_o^2 - r_1^2 \right) \right\} \ ; \text{ for step fin.} \\ \frac{4}{3}\pi \sum_{n=2,\ 4,\ \ldots}^{N} r_{n-1} \left(r_n - r_{n-1} \right) \\ \times \left(t_{n-2} + 4\ t_{n-1} + t_n \right) \ ; \text{ for non-linearly varying thickness} \\ 2\pi t_b \left(r_o^2 - r_b^2 \right) \ ; \text{ for uniform thickness} \end{cases} \tag{3.29}$$

Further, the heat transfer surface area A_s, appearing in Eq. (3.28c), is expressed by Eq. (3.30).

$$A_s = \begin{cases} 2\pi \left(r_o^2 - r_b^2 \right) + 4\pi \left\{ r_1 \left(t_1 - t_2 \right) + r_o t_2 \right\} ; \text{ for step fin.} \\ 4\pi r_o t_o + 2\pi \sum_{n=1}^{N} \left(r_n + r_{n-1} \right) \times \\ \left\{ \left(r_n - r_{n-1} \right)^2 + \left(t_{n-1} - t_n \right)^2 \right\}^{\frac{1}{2}} ; \text{ for non-linearly varying thickness} \\ 2\pi \left(r_o^2 - r_b^2 \right) + 4\pi r_o t_b \ ; \text{ for uniform thickness} \end{cases} \tag{3.30}$$

In Eqs. (3.29) and (3.30), n and (N+1) are respectively the grid index of space and total number of grid points.

3.4.3 Solution procedure

The non-dominated sorting genetic algorithm II (NSGA-II) is employed here for solving the fin design problem formulated by Eqs. (3.26) and (3.27) as multi-objective optimization models.

In the cycles of NSGA-II, the heat transfer rate, $f_1(\boldsymbol{x})$, is evaluated through Eqs. (3.5) and (3.6) for step fin, while that through Eqs. (3.12) and (3.13) for non-linearly varying and uniform thickness fins as discussed in Sections 3.1.3 and 3.3.4 respectively.

3.4.4 Numerical experimentation and discussion

In the present study, the annular fins of various profiles, namely step change in thickness, non-linearly varying thickness and uniform thickness, are analyzed in a convective and radiative environment with a constant temperature at the base of the fin and variable thermal conductivity for the fin material.

The considered operating conditions and thermal properties of the fin material along with fin geometry with reference to Figs. 3.1, 3.14 and 3.18 are listed in Table 3.6, while the user defined algorithmic parameter settings for NSGA-II are

Table 3.6: Operating conditions, fin material properties, and fin geometry of annular fins.

Parameter	Value/ Range of value
Ambient temperature, T_∞	300 K
Temperature of the fin at the base, T_b	600 K
Convective heat transfer coefficient on fin surface, h	50 W/m^{2}K
Convective heat transfer coefficient on step surface, h_s	50 W/m^{2}K
Thermal conductivity of the fin material at T_∞, k_a	186 W/mK
Parameter for variable thermal conductivity, β	-0.00018 K^{-1}
Emissivity of the fin material, ϵ	0.8
Base radius, r_b	2.0 cm
Outer radius, r_o	2.5–6.0 cm
Fin half-thickness, t (for uniform/non-linearly varying thickness fin)	0.01–0.2 cm
Radius of step change in thickness, r_1 (for step fin)	2.5–6.0 cm
Half thickness of the first step, t_1 (for step fin)	0.01–0.2 cm
Half thickness of the second step, t_2 (for step fin)	0.01–0.2 cm

given in Table 3.3. A cubic curve with open uniform knot vector and of order 4 is considered for the B-Spline curve representing the profile of the non-linearly varying thickness fin. Further, five control points are considered here to define the B-spline curve.

With the above sets of input values and randomly generated NSGA-II population, the fin design problem formulated in Eqs. (3.26) and (3.27) is studied with various combinations of the three objective functions, f_1–f_3, given by Eq. (3.28).

The Pareto fronts for the three fin profiles obtained by maximizing the heat transfer rate (f_1) and minimizing fin volume (f_2) are shown in Fig. 3.19, where the conflicting nature of the heat transfer rate and fin volume is clearly visible. It

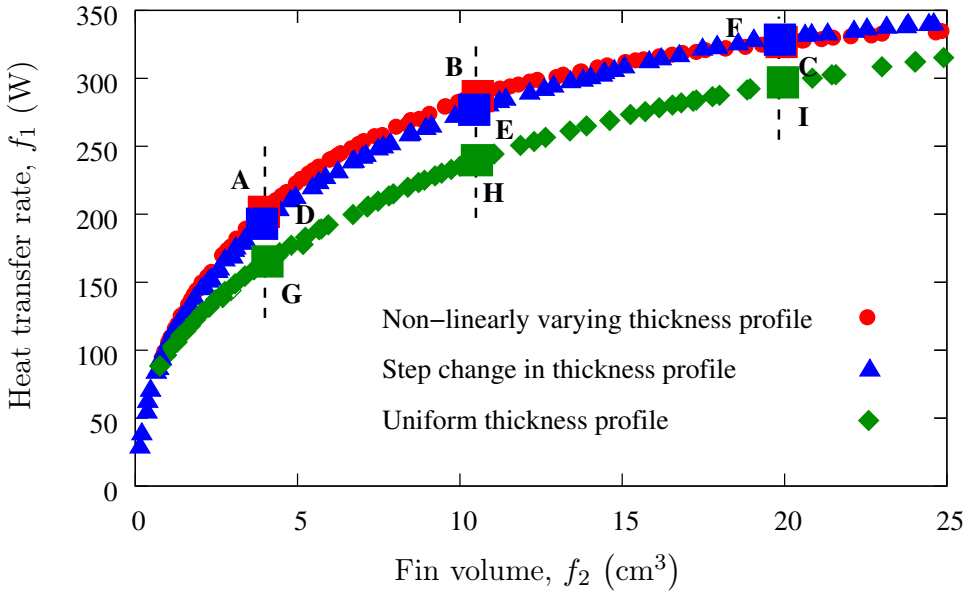

Figure 3.19: Pareto fronts of heat transfer rate versus fin volume.

is also seen in Fig. 3.19 that the non-linearly varying thickness fin has the best performance among the three profiles, followed by that of the step fin. In fact, near the end of the Pareto fronts where both the heat transfer rate and fin volume reach their maximum values, the performance of the step fin is slightly better than that of the non-linearly varying thickness fin. Nine selective efficient fin geometries (three solutions from each fin profile), corresponding to solutions A–I of Fig. 3.19, are shown in Fig. 3.20, where the patterns of significant geometric variations are clearly noticeable. For these configurations, the values of the third objective (f_3) are also computed and shown in Fig. 3.20.

For further assessment, the problem is studied in the second step for simultaneously maximizing the heat transfer rate (f_1) and fin efficiency (f_3). The obtained Pareto fronts are shown in Fig. 3.21, which reveal the conflicting nature between the heat transfer rate and fin efficiency also. It is also seen in Fig. 3.21 that the non-linearly varying thickness fin has the lowest efficiency among the three fin profiles. The Pareto fronts of the other two fins overlap with each other, indicating almost the same efficiency in both the cases. This is due to the fact that both the optimized step fin and uniform thickness fin takes almost similar shapes.

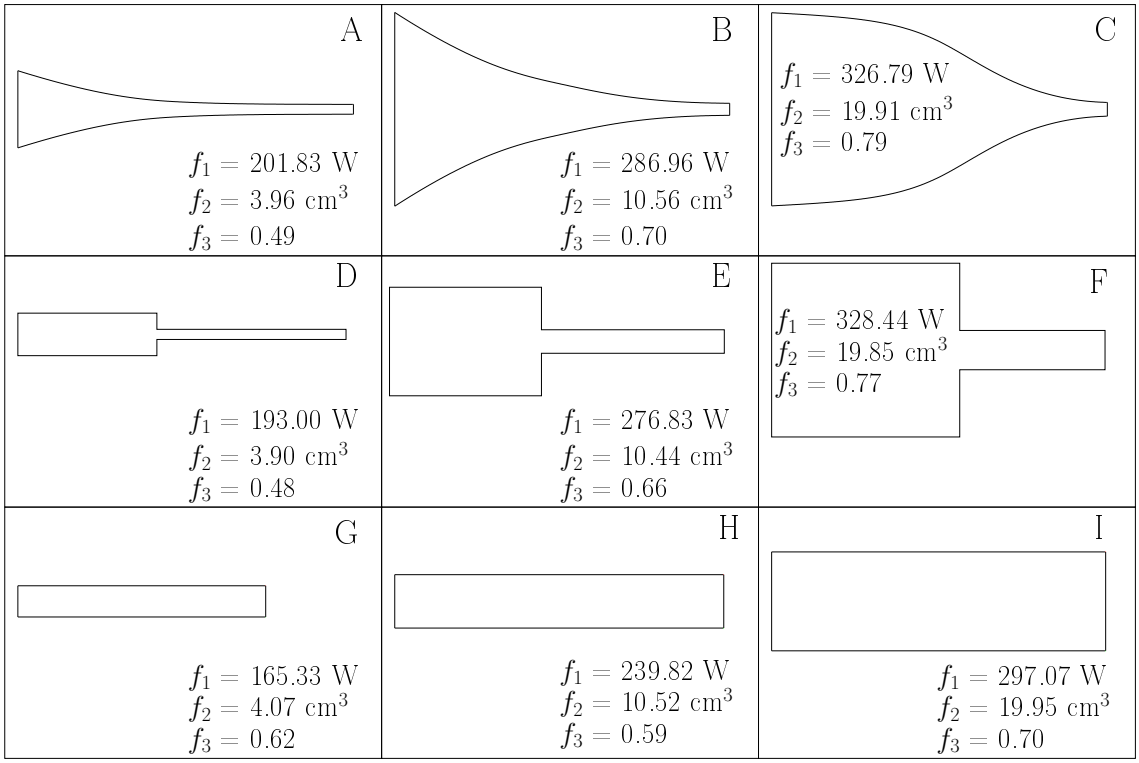

Figure 3.20: Selective fin geometries (corresponding to solutions A–I of Fig. 3.19 (a larger scale in thickness direction is used to make the variation in thickness prominent)).

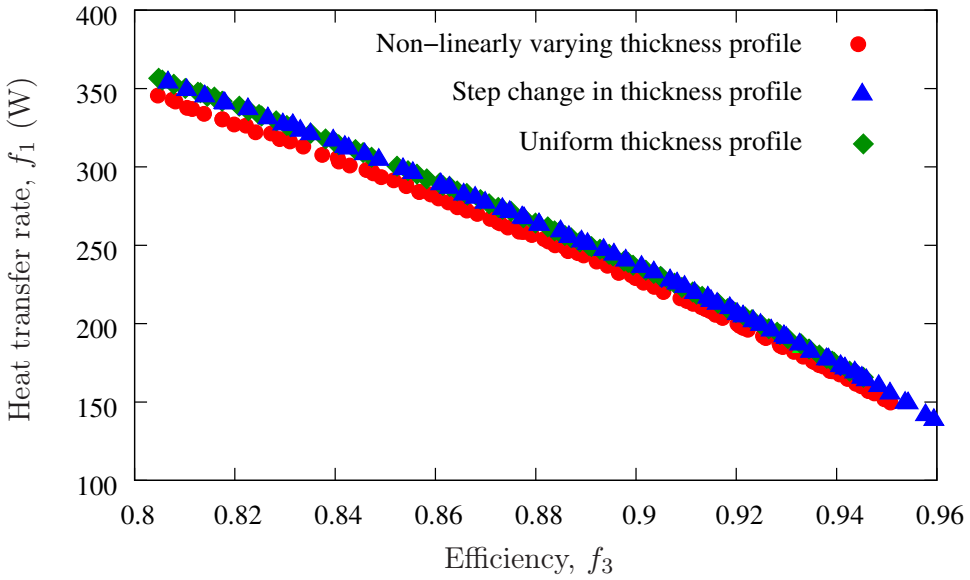

Figure 3.21: Pareto fronts of heat transfer rate versus fin efficiency.